Effects of Discretization Methods on the Performance of Resonant Controllers

Alejandro G. Yepes, *Student Member, IEEE*, Francisco D. Freijedo, *Member, IEEE*, Jesús Doval-Gandoy, *Member, IEEE*, Óscar López, *Member, IEEE*, Jano Malvar, *Student Member, IEEE*, and Pablo Fernandez-Comesaña, *Student Member, IEEE*

***Abstract*—Resonant controllers have gained significant importance in recent years in multiple applications. Because of their high selectivity, their performance is very dependent on the accuracy of the resonant frequency. An exhaustive study about different discrete-time implementations is contributed in this paper. Some methods, such as the popular ones based on two integrators, cause that the resonant peaks differ from expected. Such inaccuracies result in significant loss of performance, especially for tracking high-frequency signals, since infinite gain at the expected frequency is not achieved, and therefore, zero steady-state error is not assured. Other discretization techniques are demonstrated to be more reliable. The effect on zeros is also analyzed, establishing the influence of each method on the stability. Finally, the study is extended to the discretization of the schemes with delay compensation, which is also proved to be of great importance in relation with their performance. A single-phase active power filter laboratory prototype has been implemented and tested. Experimental results provide a real-time comparison among discretization strategies, which validate the theoretical analysis. The optimum discrete-time implementation alternatives are assessed and summarized.**

***Index Terms*—Current control, digital control, power conditioning, pulsewidth-modulated power converters, Z transforms.**

NOMENCLATURE

Variables

C	Capacitance.
f	Frequency in hertz.
$G(s)$	Model in the s domain.
$G(z)$	Model in the z domain.
$H(s)$	Resonant controller in the s domain.
$H(z)$	Resonant controller in the z domain.
i	Current.
K	Gain of resonant controller.
L	Inductance value.
m	Pulsewidth modulation (PWM) duty cycle.
N	Number of samples to compensate with computational delay compensation.
n	Highest harmonic to be compensated.
R	Equivalent series resistance value.
$R(s)$	Resonant term in the s domain.
$R(z)$	Resonant term in the z domain.
T	Period.
θ	Phase of grid voltage.
V	Voltage.
ω	Angular frequency in radians per second.
$u(s)$	Input value.
$y(s)$	Output value.

Subscripts

1	Fundamental component.
a	Actual value (f).
c	Generic current controller (G).
d	Degree of freedom in the zero-pole matching discretization method (K).
dc	Relative to the dc link (V).
f	Relative to the passive inductive filter (V, i, L, R, and G).
I	Equivalent to the double of the integral gain of a proportional + integral (PI) controller in dq frame (K).
k	Relative to the kth harmonic (H, R, K_P, and K_I).
L	Relative to the load (i).
Lh	Relative to the harmonics of the load (i).
o	Resonant frequency of a continuous resonant term or resonant controller (f and ω).
P	Equivalent to the double of the proportional gain of a PI controller in dq frame (K).
PCC	Relative to the point of common coupling (V).
PL	Relative to the plant (G).
rms	Root mean square.
s	Relative to sampling (f and T).
src	Relative to the voltage source (V, i, and L).
sw	Relative to switching (f).
T	Sum of the gains for every value of harmonic order k (K_P).
X	Resonant term R or resonant controller H discretized with method X, where $X \in \{\text{zoh}, \text{foh}, \text{f}, \text{b}, \text{t}, \text{tp}, \text{zpm}, \text{imp}\}$.
$X\&Y$	Resonant term R or resonant controller H implemented with two discrete integrators, with the direct one discretized with method X and the feedback one with method Y, where $X, Y \in \{\text{zoh}, \text{foh}, \text{f}, \text{b}, \text{t}, \text{tp}, \text{zpm}, \text{imp}\}$.

Manuscript received September 17, 2009; revised December 29, 2009. Date of current version June 18, 2010. This work was supported by the Spanish Ministry of Education and Science under Project DPI2009-07004. Recommended for publication by Associate Editor P. Mattavelli.

The authors are with the Department of Electronic Technology, University of Vigo, Vigo 36200, Spain (e-mail: agyepes@uvigo.es; fdfrei@uvigo.es; jdoval@uvigo.es; olopez@uvigo.es; janomalvar@uvigo.es; pablofercom@uvigo.es).

Color versions of one or more of the figures in this paper are available online at http://ieeexplore.ieee.org.

Digital Object Identifier 10.1109/TPEL.2010.2041256

$X-Y$	Resonant controller $H^{\mathrm{VPI}}(z)$, in which $R^1(s)$ is discretized with method X and $R^2(s)$ with method Y, where $X,Y \in \{\mathrm{zoh}, \mathrm{foh}, \mathrm{f}, \mathrm{b}, \mathrm{t}, \mathrm{tp}, \mathrm{zpm}, \mathrm{imp}\}$.
Superscripts	
$*$	Reference value.
1	Resonant term R of the form $s/(s^2+\omega_o^2)$.
2	Resonant term R of the form $s^2/(s^2+\omega_o^2)$.
d	Including delay compensation (H and R).
PR	Resonant controller H of the PR type.
VPI	Resonant controller H of the VPI type.
Others	
Δx	Difference between x and its target value (i_f).
$\hat{x}$	Estimated value of x (θ_1 and ω_1).

I. Introduction

In recent years, resonant controllers have gained significant importance in a wide range of different applications due to their overall good performance. They have been applied with satisfactory results to cases such as distributed power generation systems [1], [2], dynamic voltage regulators [3], [4], wind turbines [5], [6], photovoltaic systems [7], [8], fuel cells [9], [10], active rectifiers [11], active power filters (APFs) [12]– [17], microgrids [18], and permanent magnet synchronous motors [19].

Resonant controllers allow to track sinusoidal references of arbitrary frequencies with zero steady-state error for both single-phase and three-phase applications. An important saving of computational burden and complexity is obtained due to their implementation in stationary frame, avoiding the coordinates transformations, and providing perfect tracking of both positive and negative sequences [1], [13], [14], [20]–[22]. Resonant controllers in synchronous reference frame (SRF) have been also proposed to control pairs of harmonics simultaneously when no unbalance exist [7], [15]–[17], [22], [23].

An essential step in the implementation of resonant digital controllers is the discretization. Because of the narrow band and infinite gain of resonant controllers, they are specially sensitive to this process. Actually, a slight displacement of the resonant poles causes a significant loss of performance. In the case of proportional+resonant (PR) controllers [14], [20]–[22], even for small frequency deviations, the effect of resonant terms becomes minimal, and the PR controller behaves just as a proportional one [14]. The resonant regulator proposed in [16] is less sensitive to these variations when cross coupling due to the plant appears in the dq frame, but if these deviations in the resonant poles are present, it does not achieve zero steady-state error either. Furthermore, if selectivity is reduced to increase robustness to frequency variations, undesired frequencies and noise may be amplified. Thus, an accurate peak position is preferable to low selectivity. Therefore, it is of paramount importance to study the effectiveness of the different alternatives of discretization for implementing digital resonant controllers, due to the critical characteristics of their frequency response.

As proved in this paper, many of the existing discretization techniques cause a displacement of the poles. This fact results in a deviation of the frequency at which the infinite gain occurs with respect to the expected resonant frequency. This error becomes more significant as the sampling time and the desired peak frequency increase. In practice, it can be stated that most of these discretization methods result in suitable implementations when tracking 50/60 Hz (fundamental) references and even for low-order harmonics. However, as shown in this paper, some of them do not perform so well in applications in which signals of higher frequencies should be tracked, such as APFs and ac motor drives. This error has special relevance in the case of implementations based on two integrators, since it is a widely employed option mainly due to its simplicity for frequency adaptation [8], [13], [15], [23]–[25].

Discretization also has an effect on zeros, modifying their distribution with respect to the continuous transfer function. These discrepancies should not be ignored because they have a direct relation with stability. In fact, resonant controllers are often preferred to be based on the Laplace transform of a cosine function instead of that of a sine function because its zero improves stability [13], [19]. In a similar way, the zeros mapped by each technique will affect the stability in a different manner. Consequently, it is also convenient to establish which are the most adequate techniques from the point of view of phase versus frequency response.

However, for large values of the resonance frequency, the computational delay affects the system performance and may cause instability. Therefore, a delay compensation scheme should be implemented [14], [15], [17], [23]. It can be performed in the continuous domain as proposed in [15]. However, the discretization of that scheme leads to several different expressions. A possible implementation in the z domain was posed in [14], but there are other possibilities. Consequently, it should be analyzed how each method affects the effectiveness of the computational delay compensation. This aspect has a significant relevance since it will determine the stability at the resonant frequencies.

The study of these effects of the discretization on resonant controllers has not been analyzed in the existing literature. Therefore, it is of paramount importance to analyze how each method affects the performance in relation with these aspects.

A single-phase APF laboratory prototype has been built to check the theoretical approaches, because it is an application very suitable for proving the controllers performance when tracking different frequencies, and results can be extrapolated to other single-phase and three-phase applications where a perfect tracking/rejection of references/disturbances is sought through resonant controllers.

The paper is organized as follows. Section II presents alternative digital implementations of resonant controllers. The resonant peak displacement depending on the discretization method, as well as its influence on stability, is analyzed in Section III. Several discrete-time implementations including delay compensation, and a comparison among them, are posed in Section IV. Section V summarizes the performance of the digital implementations in each aspect and establishes the most optimum alternatives depending on the existing requirements. Finally, experimental results of Section VII validate the theoretical

analysis regarding the effects of discretization on the performance of resonant controllers.

II. Digital Implementations of Resonant Controllers

A. Resonant Controllers in the Continuous Domain

A PR controller can be expressed in the s domain as [14], [20]–[22]

$$H^{\mathrm{PR}}(s) = K_P + K_I \frac{s}{s^2+\omega_o^2} = K_P + K_I R^1(s) \quad (1)$$

with ω_o being the resonant angular frequency. $R^1(s)$ is the resonant term, which has infinite gain at the resonant frequency ($f_o = \omega_o/2\pi$). This assures perfect tracking for components rotating at f_o when implemented in closed-loop [21]. $R^1(s)$ is preferred to be the Laplace transform of a cosine function instead of that of a sine function, since the former provides better stability [13], [19].

$H^{\mathrm{PR}}(s)$ in stationary frame is equivalent to a proportional+integral (PI) controller in SRF [21]. However, if cross coupling due to the plant is present in the dq frame, undesired peaks will appear in the frequencies around f_o in closed loop [17]. This anomalous behavior worsens even more the performance when frequency deviates from its expected value. An alternative resonant regulator, known as vector PI (VPI) controller, is proposed in [16]:

$$H^{\mathrm{VPI}}(s) = \frac{K_P s^2 + K_I s}{s^2+\omega_o^2}. \quad (2)$$

The VPI controller cancels coupling terms produced when the plant has the form $1/(sL_f + R_f)$ [16], [17], [23], such as in shunt APFs and ac motor drives, with L_f and R_f being, respectively, the inductance and the equivalent series resistance of an *R–L* filter. Parameters detuning due to estimation errors in the values of L_f and R_f has been proved in [17] to have small influence on the performance.

$H^{\mathrm{VPI}}(s)$ can be decomposed as the sum of two resonant terms, $R^1(s)$ and $R^2(s)$, as follows:

$$\begin{aligned} H^{\mathrm{VPI}}(s) &= K_P \frac{s^2}{s^2+\omega_o^2} + K_I \frac{s}{s^2+\omega_o^2} \\ &= K_P R^2(s) + K_I R^1(s). \end{aligned} \quad (3)$$

Equation (3) permits to discretize $R^1(s)$ and $R^2(s)$ with different methods. In this manner, the most optimum alternative for $H^{\mathrm{VPI}}(z)$ will be the combination of the most adequate discrete-time implementation for each resonant term.

B. Implementations Based on the Continuous Transfer Function Discretization

Table I shows the most common discretization methods. The Simpson's rule approximation has not been included because it transforms a second-order function to a fourth-order one, which is undesirable from an implementation viewpoint [26].

The techniques reflected in Table I have been applied to $R^1(s)$ and $R^2(s)$, leading to the discrete mathematical expressions shown in Table II. T_s is the controller sampling period and $f_s = 1/T_s$ is the sampling rate. From Table II, it can be seen that the effect of each discretization method on the resonant poles displacement will be equal in both $R^1(s)$ and $R^2(s)$, since each method leads to the same denominator in both resonant terms.

TABLE I
Relations for Discretizing $R^1(s)$ and $R^2(s)$ by Different Methods

Discretization method	Equivalence	Notation ($i \in \{1,2\}$)
Zero-order hold	$X(z) = (1-z^{-1})Z\left\{L^{-1}\left\{\frac{X(s)}{s}\right\}\right\}$	$R^i_{\mathrm{zoh}}(z)$
First-order hold	$X(z) = \frac{(z-1)^2}{zT_s} Z\left\{L^{-1}\left\{\frac{X(s)}{s^2}\right\}\right\}$	$R^i_{\mathrm{foh}}(z)$
Forward Euler	$s = \frac{z-1}{T_s}$	$R^i_{\mathrm{f}}(z)$
Backward Euler	$s = \frac{z-1}{zT_s}$	$R^i_{\mathrm{b}}(z)$
Trapezoid (Tustin)	$s = \frac{2}{T_s}\frac{z-1}{z+1}$	$R^i_{\mathrm{t}}(z)$
Tustin with pre-warping	$s = \frac{\omega_o}{\tan(\frac{\omega_o T_s}{2})}\frac{z-1}{z+1}$	$R^i_{\mathrm{tp}}(z)$
Zero-pole matching	$z = e^{sT_s}$	$R^i_{\mathrm{zpm}}(z)$
Impulse invariant	$X(z) = Z\left\{L^{-1}\{X(s)\}\right\}$	$R^i_{\mathrm{imp}}(z)$

It should be noted that zero-pole matching (ZPM) permits a degree of freedom (K_d) to maintain the gain for a specific frequency [26].

C. Implementations Based on Two Discrete Integrators

The transfer function $H^{\mathrm{PR}}(s)$ can be discretized by decomposing $R^1(s)$ in two simple integrators, as shown in Fig. 1(a) [13]. This structure is considered advantageous when implementing frequency adaptation, since no explicit trigonometric functions are needed. Whereas other implementations require the online calculation of $\cos(\omega_o T_s)$ terms, in Fig. 1 schemes the parameter ω_o appears separately as a simple gain, so it can be modified in real time according to the actual value of the frequency to be controlled. Indeed, it is a common practice to implement this scheme due to the simplicity it permits when frequency adaptation is required [13], [15], [24], [25].

An analogous reasoning can be applied to $H^{\mathrm{VPI}}(s)$, leading to the block diagram shown in Fig. 1(b). Instead of developing an equivalent scheme to the total transfer function $H^{\mathrm{VPI}}(s)$, it could be obtained as an individual scheme for implementing each resonant term $R^1(s)$ and $R^2(s)$ could be obtained, but in this case the former is preferable because of the saving of resources.

It has been suggested in [8] to discretize the direct integrator of Fig. 1(a) scheme using forward Euler method and the feedback one using the backward Euler method. Additional alternatives of discretization for both integrators have been analyzed in [25], and it was also proposed to use Tustin for both integrators, or to discretize both with backward Euler, adding a one-step delay in the feedback line. Nevertheless, using Tustin for both integrators poses implementation problems due to algebraic loops [25]. In this paper, these proposals have been also applied to the block diagram shown in Fig. 1(b). Table III shows these three discrete-time implementations of the schemes shown in Fig. 1.

TABLE II
z-DOMAIN TRANSFER FUNCTIONS OBTAINED BY DISCRETIZING $R^1(s)$ AND $R^2(s)$ BY DIFFERENT METHODS

Discretized $R^1(s)$	Discretized $R^2(s)$
$R^1_{\text{zoh}}(z) = \frac{\sin(\omega_o T_s)}{\omega_o} \frac{z^{-1}-z^{-2}}{1-2z^{-1}\cos(\omega_o T_s)+z^{-2}}$	$R^2_{\text{zoh}}(z) = \frac{1-z^{-1}(\cos(\omega_o T_s)+1)+z^{-2}\cos(\omega_o T_s)}{1-2z^{-1}\cos(\omega_o T_s)+z^{-2}}$
$R^1_{\text{foh}}(z) = \frac{1-\cos(\omega_o T_s)}{\omega_o^2 T_s} \frac{1-z^{-2}}{1-2z^{-1}\cos(\omega_o T_s)+z^{-2}}$	$R^2_{\text{foh}}(z) = \frac{\sin(\omega_o T_s)}{\omega_o T_s} \frac{1-2z^{-1}+z^{-2}}{1-2z^{-1}\cos(\omega_o T_s)+z^{-2}}$
$R^1_{\text{f}}(z) = T_s \frac{z^{-1}-z^{-2}}{1-2z^{-1}+z^{-2}(\omega_o^2 T_s^2+1)}$	$R^2_{\text{f}}(z) = \frac{1-2z^{-1}+z^{-2}}{1-2z^{-1}+z^{-2}(\omega_o^2 T_s^2+1)}$
$R^1_{\text{b}}(z) = T_s \frac{1-z^{-1}}{(\omega_o^2 T_s^2+1)-2z^{-1}+z^{-2}}$	$R^2_{\text{b}}(z) = \frac{1-2z^{-1}+z^{-2}}{(\omega_o^2 T_s^2+1)-2z^{-1}+z^{-2}}$
$R^1_{\text{t}}(z) = 2T_s \frac{1-z^{-2}}{(\omega_o^2 T_s^2+4)+z^{-1}(2\omega_o^2 T_s^2-8)+z^{-2}(\omega_o^2 T_s^2+4)}$	$R^2_{\text{t}}(z) = 4\frac{1-2z^{-1}+z^{-2}}{(\omega_o^2 T_s^2+4)+z^{-1}(2\omega_o^2 T_s^2-8)+z^{-2}(\omega_o^2 T_s^2+4)}$
$R^1_{\text{tp}}(z) = \frac{\sin(\omega_o T_s)}{2\omega_o} \frac{1-z^{-2}}{1-2z^{-1}\cos(\omega_o T_s)+z^{-2}}$	$R^2_{\text{tp}}(z) = \cos^2(\frac{\omega_o T_s}{2}) \frac{1-2z^{-1}+z^{-2}}{1-2z^{-1}\cos(\omega_o T_s)+z^{-2}}$
$R^1_{\text{zpm}}(z) = K_d \frac{z^{-1}-z^{-2}}{1-2z^{-1}\cos(\omega_o T_s)+z^{-2}}$	$R^2_{\text{zpm}}(z) = K_d \frac{1-2z^{-1}+z^{-2}}{1-2z^{-1}\cos(\omega_o T_s)+z^{-2}}$
$R^1_{\text{imp}}(z) = T_s \frac{1-z^{-1}\cos(\omega_o T_s)}{1-2z^{-1}\cos(\omega_o T_s)+z^{-2}}$	$R^2_{\text{imp}}(z) = -\omega_o T_s \frac{z^{-1}\sin(\omega_o T_s)}{1-2z^{-1}\cos(\omega_o T_s)+z^{-2}}$

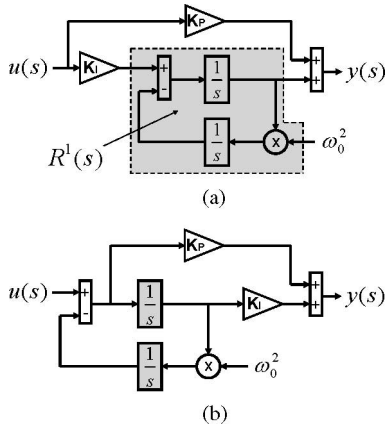

Fig. 1. Block diagrams of frequency adaptive resonant controllers (a) $H^{\text{PR}}(s)$ and (b) $H^{\text{VPI}}(s)$ based on two integrators.

It should be noted that $H^j_{\text{t\&t}}(z)$ and $H^j_t(z)$ are equivalent for both $j = \text{PR}$ and $j = \text{VPI}$, since the Tustin transformation is based on a variable substitution. The same is true for the rest of methods that consist in substituting s as a function of z. However, zero-order hold (ZOH), first-order hold (FOH), and impulse invariant methods applied separately to each integrator do not lead to H^j_{zoh}, H^j_{foh}, and H^j_{imp}, respectively. Indeed, to discretize an integrator with ZOH or FOH results in the same way as a forward Euler substitution, while to discretize an integrator with the impulse invariant is equivalent to employ backward Euler.

III. INFLUENCE OF DISCRETIZATION METHODS ON ROOTS DISTRIBUTION

A. Resonant Poles Displacement

The z domain transfer functions obtained in Section II can be grouped in the sets of Table IV, since some of them present an identical denominator, and therefore, coinciding poles.

Fig. 2 represents the pole locus of the transfer functions in Table IV. Damped resonant controllers do not assure perfect tracking [21]; poles must be placed in the unit circumference, which corresponds to a zero damping factor (infinite gain). All discretization techniques apart from A and B lead to undamped poles; the former maps the poles outside of the unit circle, whereas the latter moves them toward the origin, causing a damping factor different from zero, so both methods should be avoided. This behavior finds its explanation in the fact that these two techniques do not map the left half-plane in the s domain to the exact area of the unit circle [26].

However, there is an additional issue that should be taken into account. Although groups C, D, and E achieve infinite gain, it can be appreciated that, for an identical f_o, their poles are located in different positions of the unit circumference. This fact reveals that there exists a difference between the actual resonant frequency (f_a) and f_o, depending on the employed implementation, as also observed in Fig. 3(d). Consequently, the infinite gain may not match the frequency of the controller references, causing steady-state error.

Fig. 3(a)–(c) depicts the error $f_o - f_a$ in hertz as a function of f_o and f_s for each group. The poles displacement increases with T_s and f_o, with the exception of group E. The slope of the error is also greater as these parameters get higher.

Actually, the denominator of group D is a second-order Taylor series approximation of group E. This fact explains the increasing difference between them as the product $\omega_o T_s$ becomes larger.

Some important outcomes from this study should be highlighted.

1) The Tustin transformation, which is a typical choice in digital control due to its accuracy in most applications, features the most significant deviation in the resonant frequency.
2) The error exhibited by the methods based on two discretized integrators becomes significant even for high

TABLE III
DISCRETE TRANSFER FUNCTIONS $H^{\mathrm{PR}}(s)$ AND $H^{\mathrm{VPI}}(s)$ OBTAINED BY EMPLOYING TWO DISCRETIZED INTEGRATORS

Discretization	Discretized $H^{\mathrm{PR}}(s)$	Discretized $H^{\mathrm{VPI}}(s)$
Forward & Backward	$H^{\mathrm{PR}}_{\mathrm{f\&b}}(z) = K_P + K_I T_s \frac{z^{-1}-z^{-2}}{1+z^{-1}(\omega_o^2 T_s^2-2)+z^{-2}}$	$H^{\mathrm{VPI}}_{\mathrm{f\&b}}(z) = \frac{K_P+z^{-1}(K_I T_s-2K_P)-z^{-2}(K_I T_s-K_P)}{1+z^{-1}(\omega_o^2 T_s^2-2)+z^{-2}}$
Backward & Backward + delay	$H^{\mathrm{PR}}_{\mathrm{b\&b}}(z) = K_P + K_I T_s \frac{1-z^{-1}}{1+z^{-1}(\omega_o^2 T_s^2-2)+z^{-2}}$	$H^{\mathrm{VPI}}_{\mathrm{b\&b}}(z) = \frac{(K_I T_s+K_P)-z^{-1}(K_I T_s+2K_P)+z^{-2}K_P}{1+z^{-1}(\omega_o^2 T_s^2-2)+z^{-2}}$
Tustin & Tustin	$H^{\mathrm{PR}}_{t\&t}(z) = H^{\mathrm{PR}}_{\mathrm{t}}(z)$	$H^{\mathrm{VPI}}_{t\&t}(z) = H^{\mathrm{VPI}}_{\mathrm{t}}(z)$

TABLE IV
GROUPS OF EXPRESSIONS WITH IDENTICAL POLES IN THE z DOMAIN

Group	Expressions ($i \in \{1,2\}; j \in \{\mathrm{PR}, \mathrm{VPI}\}$)
A	$R^i_{\mathrm{f}}(z)$
B	$R^i_{\mathrm{b}}(z)$
C	$R^i_{\mathrm{t}}(z), H^j_{\mathrm{t\&t}}(z)$
D	$H^j_{\mathrm{f\&b}}(z), H^j_{\mathrm{b\&b}}(z)$
E	$R^i_{\mathrm{zoh}}(z), R^i_{\mathrm{foh}}(z), R^i_{\mathrm{tp}}(z), R^i_{\mathrm{zpm}}(z), R^i_{\mathrm{imp}}(z)$

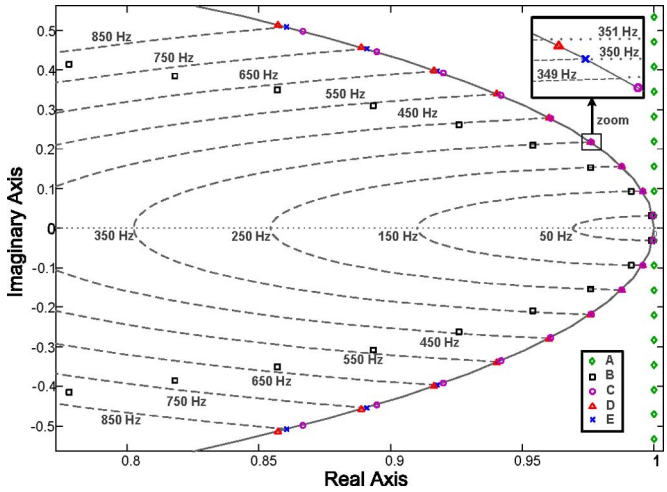

Fig. 2. Pole locus of the discretized resonant controllers at $f_s = 10$ kHz (fundamental to the 17th odd harmonics).

sampling frequencies and low-order harmonics. For instance, at $f_s = 10$ kHz, group D exhibits an error of $+0.7$ Hz for the seventh harmonic, which causes a considerable gain loss [see Fig. 3(d)]. When dealing with higher harmonic orders (h), such as 13 and 17, it raises to 4.6 and 10.4 Hz, respectively, which is unacceptable.

3) Group E leads to poles that match the original continuous ones, so the resonant peak always fits the design frequency f_o.

B. Effects on Zeros Distribution

Once assured infinite gain due to a correct position of the poles, another factor to take into account is the displacement of zeros caused by the discretization. Resonant controllers that belong to group E have been proved to be more suitable for an optimum implementation in terms of resonant peak displacement. However, the numerators of these discrete transfer functions are not the same, and they depend on the discretization method. This aspect has a direct relation with stability, so it should not be ignored.

On the other hand, although group D methods produce a resonant frequency error, they avoid the calculation of explicit cosine functions when frequency adaptation is needed. This fact may imply an important saving of resources. Therefore, it is also of interest to establish which is the best option of that set.

The analysis will be carried out by means of the frequency response. The infinite gain at ω_o is given by the poles position, whereas zeros only have a visible impact on the gain at other frequencies. Concerning phase, the mapping of zeros provided by the discretization may affect all the spectrum, including the phase response near the resonant frequency. Due to the high gain around ω_o, the phase introduced by the resonant terms at $\omega \approx \omega_o$ will have much more impact on the phase response of the whole controllers than at the rest of the spectrum [14]. Therefore, the influence of discretization on the stability should be studied mainly by analyzing the phase lag caused at $\omega \approx \omega_o$.

1) Displacement of $R^1(s)$ Zeros by Group E Discretizations: Fig. 4 compares the frequency response of a resonant controller $R^1(s)$, designed for the seventh harmonic, when discretization methods of group E are employed at $f_s = 10$ kHz. An almost equivalent magnitude behavior is observed, even though $R^1_{\mathrm{imp}}(z)$ has a lower attenuation in the extremes, and both $R^1_{\mathrm{tp}}(z)$ and $R^1_{\mathrm{foh}}(z)$ tend to reduce the gain at high frequencies. However, the phase versus frequency plot differs more significantly.

From Fig. 4, it can be appreciated that $R^1_{\mathrm{tp}}(z)$ and $R^1_{\mathrm{foh}}(z)$ are the most accurate when comparing with $R^1(s)$. On the contrary, the phase lag introduced by $R^1_{\mathrm{zoh}}(z)$ and $R^1_{\mathrm{zpm}}(z)$ is higher than for the continuous model. This fact is particularly critical at $\omega \approx \omega_o$, even though they also cause delay for higher frequencies. As shown in Fig. 4, they introduce a phase lag at $f_o = 350$ Hz of 6.3°. For higher values of $\omega_o T_s$, it becomes greater. For instance, if tuned at a resonant frequency of $f_o = 1750$ Hz with $f_s = 10$ kHz, the delay is 32°. Therefore, the implementation of $R^1_{\mathrm{zoh}}(z)$ and $R^1_{\mathrm{zpm}}(z)$ may lead to instability. On the other hand, $R^1_{\mathrm{tp}}(z)$, $R^1_{\mathrm{foh}}(z)$, and $R^1_{\mathrm{imp}}(z)$ accurately reproduce the frequency response at the resonance frequency, maintaining the stability of the continuous controller at ω_o. Fig. 4 also shows that $R^1_{\mathrm{imp}}(z)$ can be considered the most advantageous implementation of $R^1(s)$, since it maintains the stability at $\omega \approx \omega_o$ and introduces less phase lag in open-loop for the rest of the spectrum, thereby allowing for a larger phase margin.

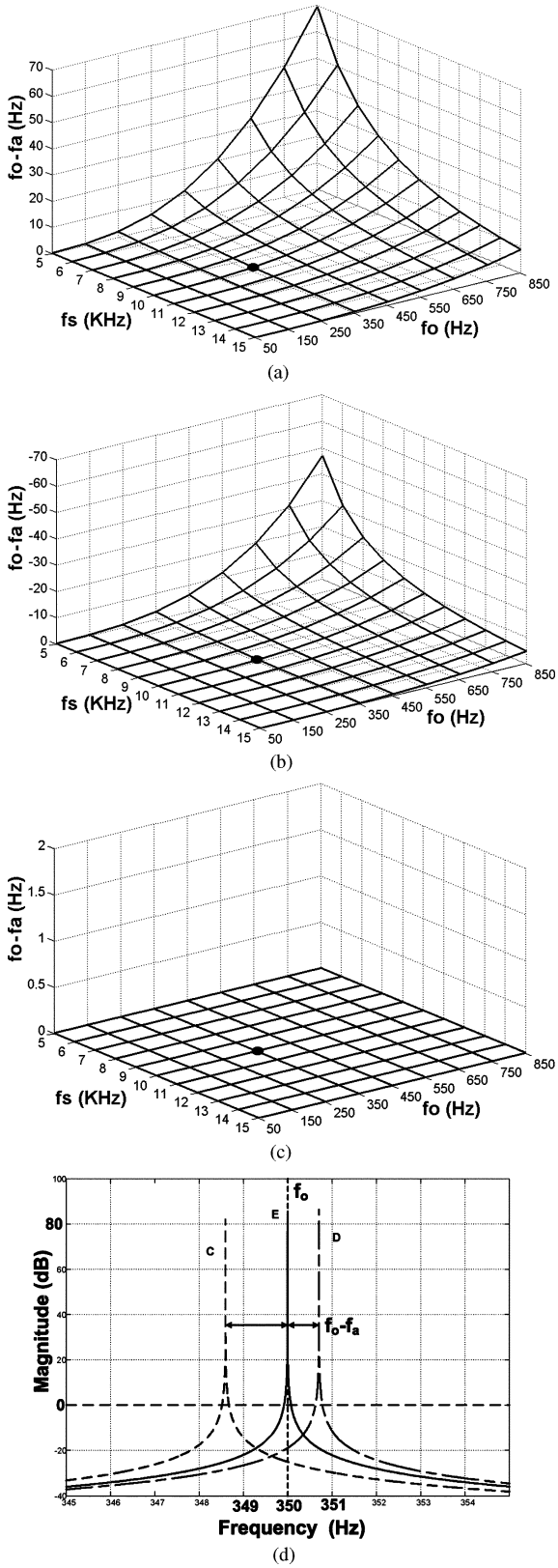

Fig. 3. Deviation of the resonance frequency of the discretized controller f_a from the resonance frequency f_o of the continuous controller. (a) Group C transfer functions. (b) Group D transfer functions. (c) Group E transfer functions. (d) Discretized seventh harmonic resonant resonant controller at $f_s = 10$ kHz.

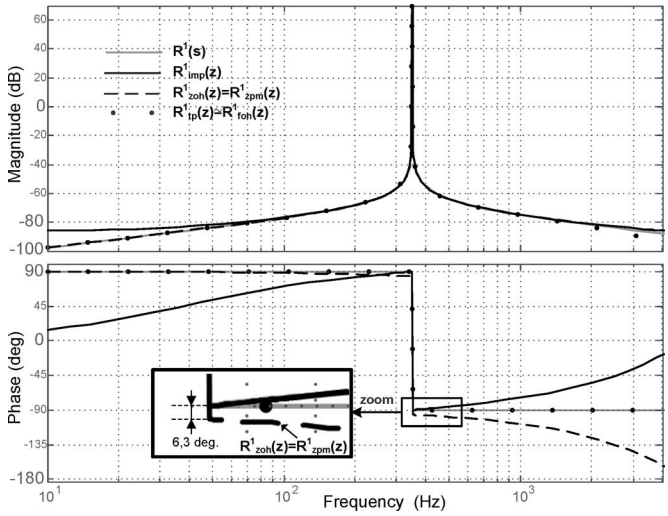

Fig. 4. Bode plot of $R^1(s)$ discretized with group E methods for a seventh harmonic resonant controller at $f_s = 10$ kHz.

In any case, the influence of the discretization at $\omega \neq \omega_o$ is not as important as its effect on the stability at $\omega \approx \omega_o$, since the gain of $R^1(z)$ is much lower at those frequencies. Consequently, this aspect can be neglected unless low sample frequencies, high resonant frequencies, and/or large values of K_I/K_P are employed. In these cases, it can be taken into account in order to avoid unexpected reductions in the phase margin that could affect the stability, or even to increase its value over the phase margin of the continuous system by means of $R^1_{\rm imp}(z)$.

2) Displacement of $R^2(s)$ Zeros by Group E Discretizations: The frequency response of $R^2(s)$ discretizations is shown in Fig. 5(a). It can be seen that ZOH produces a phase lag near the resonant frequency that could affect stability.

Among the rest of possibilities of group E, the impulse invariant method is also quite unfavorable: it provides much less gain after the resonant peak than the rest of the discretizations. This fact causes that the zero phase provided by $R^2(z)$ for $\omega > \omega_o$ has much less impact on the global transfer function $H^{\rm VPI}(z)$, in comparison to the phase delay introduced by $R^1(z)$. In this manner, the phase response of $H^{\rm VPI}(z)$ would show a larger phase lag if $R^2(s)$ is discretized with impulse invariant instead of other methods, worsening the stability at $\omega > \omega_o$.

Actually, as shown in Fig. 5(b), if $R^2_{\rm imp}(z)$ is used, the delay of $H^{\rm VPI}(z)$ can become close to -45° for certain frequencies, which is certainly not negligible. This is illustrated, as an example, in Fig. 5(b), in which Bode plot of $H^{\rm VPI}(z)$ is shown when it is implemented as $R^1_{\rm imp}(z)$, and $R^2(s)$ is discretized with the different methods. Fixed values of K_I and K_P have been employed to make the comparison possible. $K_I = K_P\ R_f/L_f$ has been chosen, so the cross coupling due to the plant is canceled [16], [17], and an arbitrary value of 1 has been assigned to K_P as an example. According to the real parameters of the laboratory prototype, $L_f = 5$ mH and $R_f = 0.5\ \Omega$. If the ratio K_I/K_P is changed, the differences will become more or less notable, but essentially, each method will still affect in the same manner. It should be remarked that the phase response

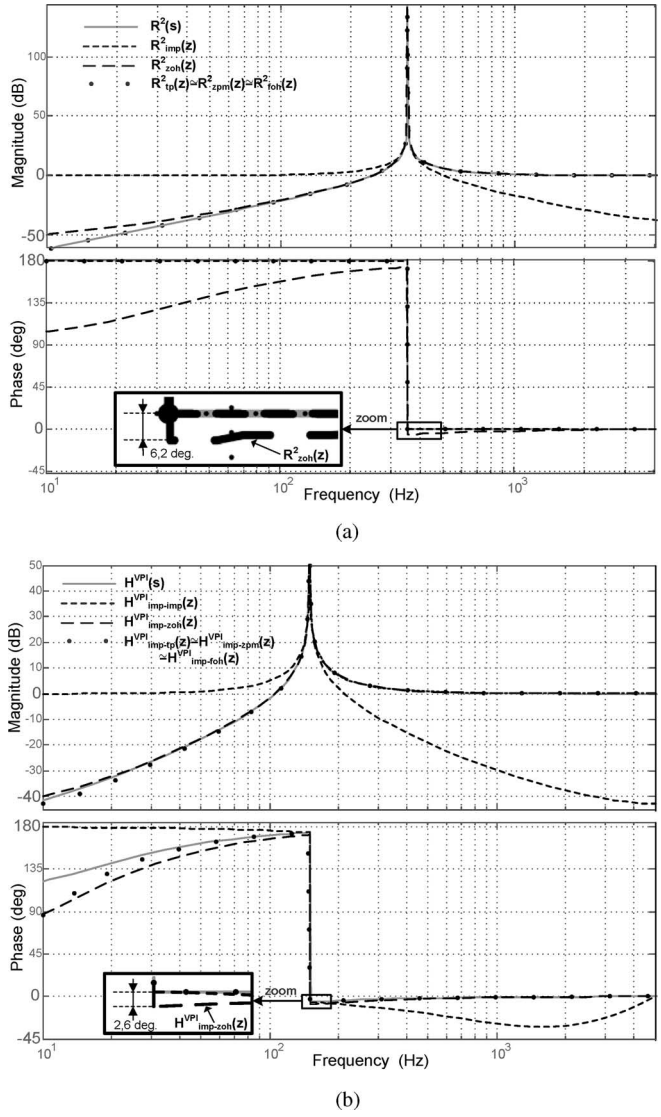

Fig. 5. Study of group E discretizations effect on $R^2(s)$ zeros. (a) Frequency response of $R^2(s)$ discretized with group E methods for a seventh harmonic resonant controller at $f_s = 10$ kHz. (b) Frequency response of $H^{\mathrm{VPI}}(z)$ for a third harmonic resonant controller at $f_s = 10$ kHz, with $R^1_{\mathrm{imp}}(z)$, when $R^2(s)$ is discretized by each method of group E. $K_P = 1$ and $K_I = K_P R_f / L_f$, with $R_f = 0.5\ \Omega$ and $L_f = 5$ mH.

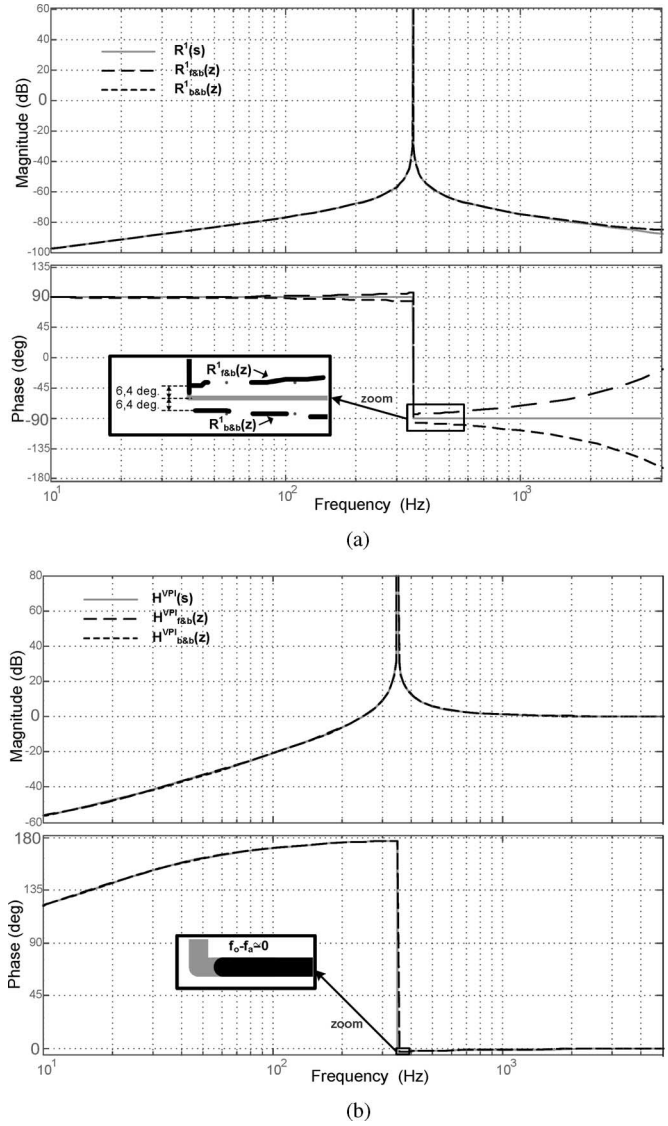

Fig. 6. Frequency response of $R^1(s)$ and $H^{\mathrm{VPI}}(s)$ implemented with group D methods for a seventh harmonic resonant controller at $f_s = 10$ kHz. (a) $R^1(s)$. (b) $H^{\mathrm{VPI}}(s)$, $K_P = 1$, and $K_I = K_P R_f / L_f$, with $R_f = 0.5\ \Omega$ and $L_f = 5$ mH.

of $H^{\mathrm{VPI}}(z)$ at $\omega \approx \omega_o$ is not modified by $R^1_{\mathrm{imp}}(z)$, but only by the discretization of $R^2(s)$. Fig. 5(b) also shows that some implementations introduce less phase at low frequencies than $H^{\mathrm{VPI}}(s)$, but the influence of this aspect on the performance can be neglected.

In conclusion, any of the discretization methods of group E, with the exception of impulse invariant and ZOH, are adequate for the implementation of $R^2(z)$. Actually, the influence of these two methods is so negative that they could easily lead to instability continuous resonant controllers with considerable stability margins.

3) Displacement of Zeros by Group D Discretizations: Fig. 6(a) shows the Bode plot of $R^1(s)$ implemented with set D schemes. $R^1_{\mathrm{f\&b}}(z)$ produces a phase lead in comparison to $R^1(s)$, whereas $R^1_{\mathrm{b\&b}}(z)$ causes a phase lag. This is also true at $\omega \approx \omega_o$, which are the most critical frequencies. Therefore, $R^1_{\mathrm{f\&b}}(z)$ is preferable to $R^1_{\mathrm{b\&b}}(z)$. On the other hand, as can be appreciated in Fig. 6(b), the Bode plot of $H^{\mathrm{VPI}}_{\mathrm{f\&b}}(z)$ and $H^{\mathrm{VPI}}_{\mathrm{b\&b}}(z)$ scarcely differ. They both achieve an accurate reproduction of $H^{\mathrm{VPI}}(s)$ frequency response. Actually, at $\omega \approx \omega_o$, they provide exactly the same phase. Consequently, they can be indistinctly employed with satisfactory results.

IV. Discretization Influence on Computational Delay Compensation

A. Delay Compensation in the Continuous Domain

For large values of ω_o, the delay caused by T_s affects the system performance and may cause instability. Therefore, a delay

compensation scheme should be implemented [14], [15], [17], [23], [27].

1) Delay Compensation for $H^{\mathrm{PR}}(s)$: Concerning resonant controllers based on the form $H^{\mathrm{PR}}(s)$, a proposal was posed in [15] for performing the compensation of the computational delay. The resulting transfer function can be expressed in the s domain as

$$H^{\mathrm{PR}^d}(s) = K_P + K_I \frac{s\cos(\omega_o N T_s) - \omega_o \sin(\omega_o N T_s)}{s^2 + \omega_o^2} = K_P + K_I R^{1^d} \tag{4}$$

with N being the number of sampling periods to be compensated. According to the work of Limongi *et al.* [23], $N = 2$ is the most optimum value.

2) Delay Compensation for $H^{\mathrm{VPI}}(s)$: Because of $H^{\mathrm{VPI}}(s)$ superior stability, it only requires computational delay for much greater resonant frequencies than $H^{\mathrm{PR}}(s)$ [16], [17], [23]. Delay compensation could be obtained by selecting $K_P = \cos(\omega_o N T_s)$ and $K_I = -\omega_o \sin(\omega_o N T_s)$. However, this approach would not permit to choose the parameters so as to satisfy $K_I/K_P = R_f/L_f$; thus, it would not cancel the cross coupling terms as proposed in [16] and [17].

Therefore, an alternative approach is proposed shortly. $R^{1^d}(s)$ and $R^{2^d}(s)$ are individually implemented with a delay compensation of N samples each, so K_P and K_I can be still adjusted in order to cancel the plant pole:

$$H^{\mathrm{VPI}^d}(s) = K_P \frac{s^2\cos(\omega_o N T_s) - s\omega_o \sin(\omega_o N T_s)}{s^2 + \omega_o^2} + K_I \frac{s\cos(\omega_o N T_s) - \omega_o \sin(\omega_o N T_s)}{s^2 + \omega_o^2} = K_P R^{2^d} + K_I R^{1^d}. \tag{5}$$

3) Delay Compensation for $R^{1^d}(s)$ and $R^{2^d}(s)$: If the resonant terms are decomposed by the use of two integrators, it is possible to perform the delay compensation by means of the block diagrams depicted in Fig. 7(a) and (b) for $R^{1^d}(s)$ and $R^{2^d}(s)$, respectively.

Fig. 8 illustrates the effect of the computational delay compensation for both $R^{1^d}(s)$ and $R^{2^d}(s)$, setting $f_o = 350$ Hz and $f_s = 10$ kHz as an example. As N increases, the 180° phase shift at f_o rises, compensating the phase lag that would be caused by the delay.

B. Discrete-Time Implementations of Delay Compensation Schemes

As stated in the previous section, the delay compensation should be implemented for each resonant term separately. For this reason, it is convenient to study how each discretization method affects the effectiveness of the delay compensation for $R^{1^d}(z)$ and $R^{2^d}(z)$ individually. Effects on groups E and D implementations, due to their superior performance, are analyzed. Tables V and VI reflect the discrete transfer functions obtained by the application of these methods to $R^{1^d}(s)$ and $R^{2^d}(s)$, respectively. $R^{1^d}_{\mathrm{f\&b}}(z)$ and $R^{1^d}_{\mathrm{b\&b}}(z)$ result of applying the corresponding discretization transforms to the scheme shown in Fig. 7(a). On the other hand, $R^{2^d}_{\mathrm{f\&b}}(z)$ and $R^{2^d}_{\mathrm{b\&b}}(z)$ are obtained by discretizing the integrators shown in Fig. 7(b).

Substituting $N = 0$ in Tables V and VI leads to the expressions of Tables II and III, respectively. It can be also noted that

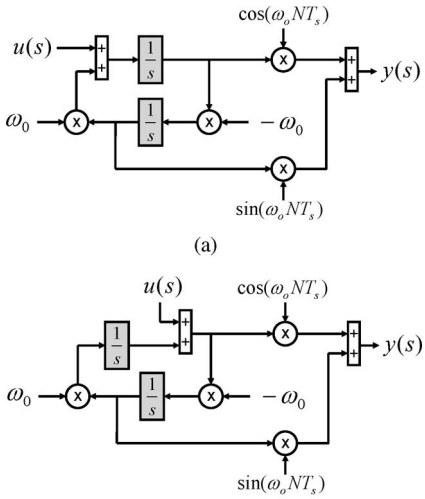

Fig. 7. Implementations of (a) $R^{1^d}(s)$ and (b) $R^{2^d}(s)$ based on two integrators.

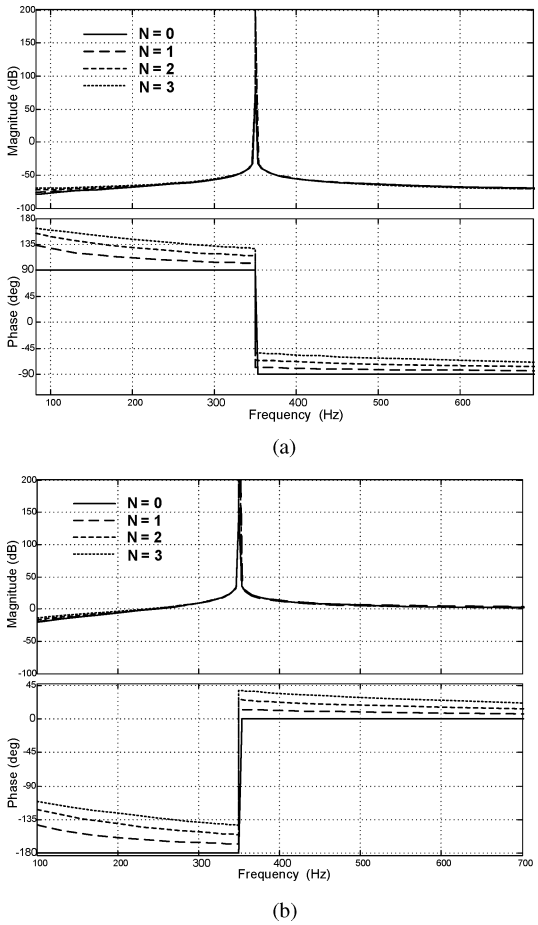

Fig. 8. Frequency response of (a) $R^{1^d}(s)$ and (b) $R^{2^d}(s)$ for different values of N; $f_o = 350$ Hz and $f_s = 10$ kHz.

TABLE V
$R^{1^d}(s)$ DISCRETIZED BY GROUPS E AND D

Zero order hold	$R^{1d}_{\text{zoh}}(z) = \frac{z^{-1}[\sin(\omega_o T_s(N+1)) - sin(\omega_o NT_s)] + z^{-2}[\sin(\omega_o T_s(N-1)) - sin(\omega_o NT_s)]}{\omega_o(1-2z^{-1}\cos(\omega_o T_s)+z^{-2})}$
First order hold	$R^{1d}_{\text{foh}}(z) = \frac{(1-z^{-2})\{\cos(\omega_o NT_s)+\sin(\omega_o NT_s)\omega_o T_s - \cos(\omega_o T_s(N+1))\} + 2z^{-1}\sin(\omega_o NT_s)[\sin(\omega_o T_s) - \cos(\omega_o T_s)]}{\omega_o^2 T_s(1-2z^{-1}\cos(\omega_o T_s)+z^{-2})}$
Tustin with prewarping	$R^{1d}_{\text{tp}}(z) = \frac{\frac{1}{2}(1-z^{-2})\cos(\omega_o NT_s)\sin(\omega_o T_s) - (1+2z^{-1}+z^{-2})\sin(\omega_o NT_s)\sin^2(\frac{\omega_o T_s}{2})}{\omega_o(1-2z^{-1}\cos(\omega_o T_s)+z^{-2})}$
Zero-pole matching	$R^{1d}_{\text{zpm}}(z) = K_d \frac{z^{-1} - z^{-2}e^{(\tan(\omega_o NT_s)\omega_o T_s)}}{1-2z^{-1}\cos(\omega_o T_s)+z^{-2}}$
Impulse invariant	$R^{1d}_{\text{imp}}(z) = T_s \frac{cos(\omega_o NT_s) - z^{-1}\cos(\omega_o T_s(N-1))}{1-2z^{-1}\cos(\omega_o T_s)+z^{-2}}$
Forward & Backward	$R^{1d}_{\text{f\&b}}(z) = T_s \frac{z^{-1}[\cos(\omega_o NT_s) - \omega_o T_s \sin(\omega_o NT_s)] - z^{-2}\cos(\omega_o NT_s)}{1+z^{-1}(\omega_o^2 T_s^2 - 2)+z^{-2}}$
Backward & Backward	$R^{1d}_{\text{b\&b}}(z) = T_s \frac{\cos(\omega_o NT_s) - z^{-1}[\cos(\omega_o NT_s) + \omega_o T_s \sin(\omega_o NT_s)]}{1+z^{-1}(\omega_o^2 T_s^2 - 2)+z^{-2}}$

TABLE VI
$R^{2^d}(s)$ DISCRETIZED BY GROUPS E AND D

Zero order hold	$R^{2d}_{\text{zoh}}(z) = \frac{(1-z^{-1})\cos(\omega_o NT_s) - (z^{-1}-z^{-2})\cos(\omega_o T_s(N-1))}{1-2z^{-1}\cos(\omega_o T_s)+z^{-2}}$
First order hold	$R^{2d}_{\text{foh}}(z) = \frac{[\sin(\omega_o T_s(N+1)) - \sin(\omega_o NT_s)] - 2z^{-1}\sin(\omega_o T_s)\cos(\omega_o NT_s) + z^{-2}[\sin(\omega_o T_s(1-N)) + sin(\omega_o NT_s)]}{\omega_o T_s(1-2z^{-1}\cos(\omega_o T_s)+z^{-2})}$
Tustin with prewarping	$R^{2d}_{\text{tp}}(z) = \frac{\frac{1}{2}(-1+z^{-2})\sin(\omega_o T_s)\sin(\omega_o NT_s) + (1-2z^{-1}+z^{-2})\cos^2(\frac{\omega_o T_s}{2})\cos(\omega_o NT_s)}{1-2z^{-1}\cos(\omega_o T_s)+z^{-2}}$
Zero-pole matching	$R^{2d}_{\text{zpm}}(z) = K_d \frac{1-z^{-1}[1+e^{(\tan(\omega_o NT_s)\omega_o T_s)}] + z^{-2}e^{(\tan(\omega_o NT_s)\omega_o T_s)}}{1-2z^{-1}\cos(\omega_o T_s)+z^{-2}}$
Impulse invariant	$R^{2d}_{\text{imp}}(z) = \omega_o T_s \frac{-\sin(\omega_o NT_s) + z^{-1}\sin(\omega_o T_s(N-1))}{1-2z^{-1}\cos(\omega_o T_s)+z^{-2}}$
Forward & Backward	$R^{2d}_{\text{f\&b}}(z) = \frac{(1-2z^{-1}+z^{-2})\cos(\omega_o NT_s) - (z^{-1}-z^{-2})\omega_o T_s \sin(\omega_o NT_s)}{1+z^{-1}(\omega_o^2 T_s^2 - 2)+z^{-2}}$
Backward & Backward	$R^{2d}_{\text{b\&b}}(z) = \frac{(1-2z^{-1}+z^{-2})\cos(\omega_o NT_s) - (1-z^{-1})\omega_o T_s \sin(\omega_o NT_s)}{1+z^{-1}(\omega_o^2 T_s^2 - 2)+z^{-2}}$

$R^{1d}_{\text{imp}}(z)$ is equivalent to the proposals of Yuan *et al.* [14] for digital implementation of the computational delay.

C. Study of Discretization Effects on Delay Compensation

To quantify the influence of each discretization technique on the desired delay compensation, an error function is defined as follows:

$$\text{Error} = \lim_{\omega \to \omega_o} \left(\angle R^{i^d}(s) - \angle R^{i^d}_X(z) \right) \tag{6}$$

for each discretization method X, with $i \in \{1, 2\}$. This parameter reflects the difference in degrees between the expected and the actual phase lead introduced. It can be evaluated as a function of f_s, N, and ω_o. Figs. 9 and 10 show the resulting values of applying the error function to discretization methods E and D, respectively.

Since the variables T_s and ω_o always appear together in the expressions as a product, both parameters have an analogous impact on the delay compensation. In this manner, the error increases with T_s with the same rate of change as with ω_o.

Fig. 9(a) represents the error function (6) evaluated in the cases of $R^{1d}_{\text{zoh}}(z)$ and $R^{2d}_{\text{zoh}}(z)$. It assumes large values for most combinations of T_s and ω_o, so these discretizations are not appropriate. It should be also noted that, for $R^{1d}_{\text{zoh}}(z)$ and $R^{2d}_{\text{zoh}}(z)$, the error is independent of N.

On the other hand, as illustrated in Fig. 9(b), three of the considered discretization methods provide an accurate delay compensation for both resonant terms: impulse invariant, Tustin with prewarping, and FOH.

From Fig. 9(c) and (d), it can be appreciated that the ZPM method is not recommendable for discretizing neither $R^{1^d}(s)$ nor $R^{2^d}(s)$. Indeed, it provides the largest phase error. It is interesting to note that, on the contrary, ZPM is adequate for $R^2(s)$ when delay compensation is not included (proved in Section III). This result is also confirmed by the surface $N = 0$ shown in Fig. 9(d).

Fig. 9 illustrates that, for E methods, the discrepancy is more significant as ω_o is higher. This is really important since the effect of delay compensation must be taken into account for high resonant frequencies. Concerning group D implementations, they do not always lead to a positive slope $\partial\text{Error}/\partial\omega_o$; for certain intervals, as shown in Fig. 10, the opposite is true. In any case, the error is of great magnitude in both groups for most values of T_s and ω_o.

It can be observed in Fig. 10(a) and (c) that $R^{1d}_{\text{b\&b}}$ and $R^{2d}_{\text{b\&b}}$ introduce a phase lead greater than the continuous controller.

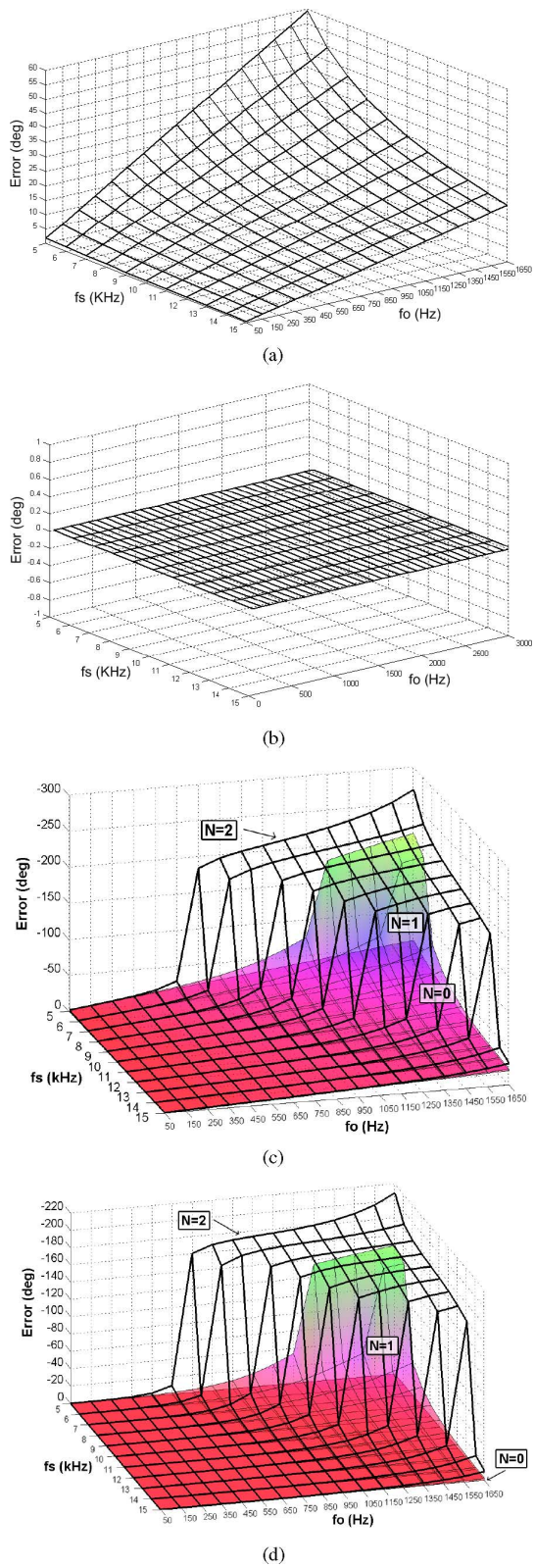

Fig. 9. Study of the error in degrees between the discretized and the continuous phase within a vicinity of the resonant frequency, for $R^{1^d}(s)$ and $R^{2^d}(s)$ discretized with group E methods. (a) $R^{1d}_{\mathrm{zoh}}(z)$ and $R^{2d}_{\mathrm{zoh}}(z)$. The same error is obtained for $N = 0, 1, 2$. (b) $R^{1d}_{\mathrm{foh}}(z)$, $R^{1d}_{\mathrm{tp}}(z)$, $R^{1d}_{\mathrm{imp}}(z)$, $R^{2d}_{\mathrm{foh}}(z)$, $R^{2d}_{\mathrm{tp}}(z)$, and $R^{2d}_{\mathrm{imp}}(z)$. The same error is obtained for $N = 0, 1, 2$. (c) $R^{1d}_{\mathrm{zpm}}(z)$. (d) $R^{2d}_{\mathrm{zpm}}(z)$.

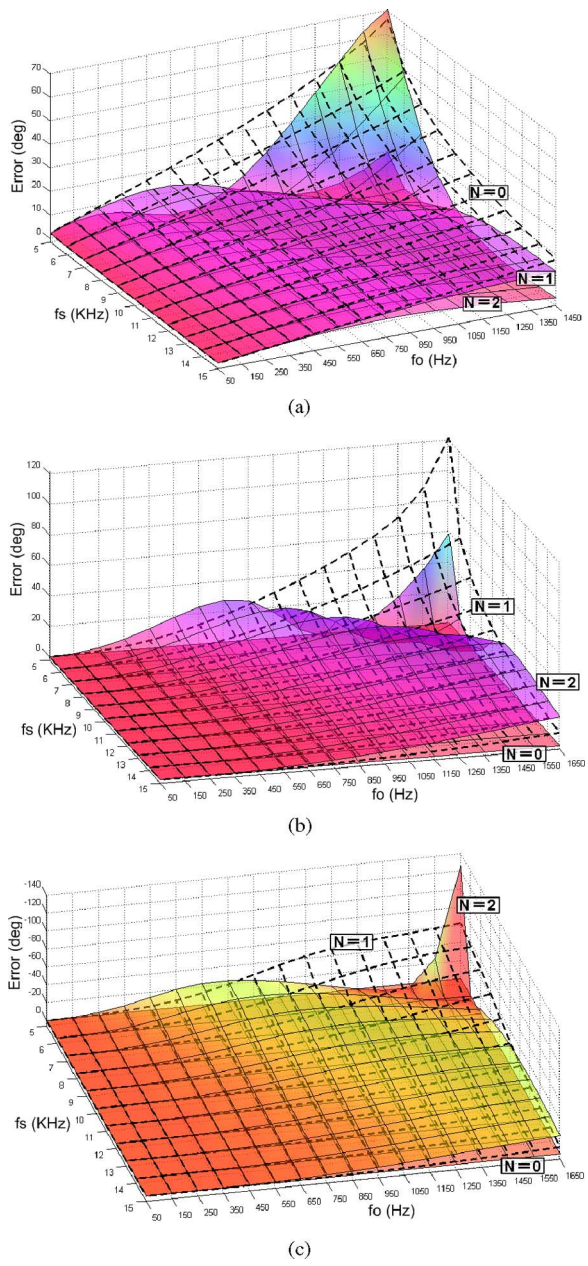

Fig. 10. Study of the error in degrees between the discretized and the continuous phase within a vicinity of the resonant frequency for $R^{1^d}(s)$ and $R^{2^d}(s)$ discretized with group D methods. (a) $R^{1d}_{\mathrm{f\&b}}(z)$. The error of $R^{1d}_{\mathrm{b\&b}}(z)$ is the opposite. (b) $R^{2d}_{\mathrm{f\&b}}(z)$. (c) $R^{2d}_{\mathrm{b\&b}}(z)$. Note that Error < 0.

This fact is preferable to the cases of $R^{1d}_{\mathrm{f\&b}}$ and $R^{2d}_{\mathrm{f\&b}}$, in which stability is reduced by a phase lag, as depicted, respectively, in Fig. 10(a) and 10(b). Nevertheless, the positive phase difference is actually so large that it could also lead to an unstable system. For these reasons, group D methods should be avoided if delay compensation is needed.

In sum, the only methods that provide an accurate discretization of delay compensation schemes are, for either resonant term, the impulse invariant, Tustin with prewarping, or FOH transforms.

TABLE VII
PERFORMANCE OF THE DISCRETE-TIME IMPLEMENTATIONS

Implementations	Infinite gain	Resonance deviation	Effect on zeros	Delay compensation	Trig. terms	References
$R^1_{\rm f}(z), R^1_{\rm b}(z), R^2_{\rm f}(z), R^2_{\rm b}(z)$	No	-	-	-	No	-
$R^1_{\rm t}(z), H^{\rm PR}_{\rm t\&t}(z), R^2_{\rm t}(z), H^{\rm VPI}_{\rm t\&t}(z)$	Yes	Very Large	-	-	No	[25], [28]
$H^{\rm PR}_{\rm b\&b}(z)$	Yes	Large	Phase lag at ω_o	Not effective	No	[25]
$H^{\rm PR}_{\rm f\&b}(z)$	Yes	Large	Phase lead at ω_o	Not effective	No	[8], [25]
$H^{\rm VPI}_{\rm f\&b}(z), H^{\rm VPI}_{\rm b\&b}(z)$	Yes	Large	Accurate	Not effective	No	-
$R^1_{\rm zoh}(z), R^1_{\rm zpm}(z), R^2_{\rm zoh}(z)$	Yes	No	Phase lag at ω_o	Not effective	Yes	-
$R^2_{\rm zpm}(z)$	Yes	No	Accurate	Not effective	Yes	-
$R^1_{\rm imp}(z)$	Yes	No	Accurate at ω_o and phase lead at $\uparrow \omega$	Accurate	Yes	-
$R^2_{\rm imp}(z)$	Yes	No	Accurate at ω_o and phase lag at $\uparrow \omega$	Accurate	Yes	-
$R^1_{\rm foh}(z), R^1_{\rm tp}(z), R^2_{\rm foh}(z), R^2_{\rm tp}(z)$	Yes	No	Accurate	Accurate	Yes	[24], [29]–[31]

TABLE VIII
OPTIMUM DISCRETE-TIME IMPLEMENTATIONS

	No frequency adaptation	**Frequency adaptation**	
		$\uparrow f_s, \downarrow \omega_o$	$\downarrow f_s, \uparrow \omega_o$
No delay comp.	$H^{\rm PR}_{\rm imp}(z)$ $H^{\rm VPI}(z) = K_P \cdot R^2_{foh,tp,zpm}(z) + K_I \cdot R^1_{\rm imp}(z)$	$H^{\rm PR}_{\rm f\&b}(z)$ $H^{\rm VPI}_{\rm f\&b}(z),\ H^{\rm VPI}_{\rm b\&b}(z)$	$*H^{\rm PR}_{\rm imp}(z)$ $*H^{\rm VPI}(z) = K_P \cdot R^2_{foh,tp,zpm}(z) + K_I \cdot R^1_{\rm imp}(z)$
Delay comp.	$H^{{\rm PR}^d}_{\rm imp}(z)$ $H^{{\rm VPI}^d}(z) = K_P \cdot R^{2^d}_{foh,tp}(z) + K_I \cdot R^{1^d}_{\rm imp}(z)$	$*H^{{\rm PR}^d}_{\rm imp}(z)$ $*H^{{\rm VPI}^d}(z) = K_P \cdot R^{2^d}_{foh,tp}(z) + K_I \cdot R^{1^d}_{\rm imp}(z)$	

* Requires the online computation of $\cos(\omega_o T_s)$ terms as ω_o varies.

V. SUMMARY OF OPTIMUM DISCRETE-TIME IMPLEMENTATIONS

Table VII summarizes the performance of the implementations in each of the aspects that have been carried out in the previous sections. The second and third columns correspond to Section III-A, the fourth column corresponds to Section III-B, and the fifth one corresponds to Section IV. Table VII also indicates which alternatives include explicit trigonometric functions in their difference equations, which lead to a higher computational burden if they are calculated online (frequency adaptation). Finally, the last column points out some previous works that employ certain implementations.

Different situations and requirements may arise when dealing with real applications. Table VIII shows the best tradeoff alternatives for discrete-time implementation depending on which are the specific requirements of a particular application.

It is known that one of the most important drawbacks of resonant regulators is their sensitiveness to frequency variations of the signal to be controlled [2], [32]. Many of the existing proposals for frequency adaptation of resonant controllers rely on discretizing two separated integrators (defined as group D in Section II-C) [8], [24], [25]. Their main advantage is the fact that they do not require the online computation of explicit cosine functions. However, these schemes cause an error in the frequency at which the resonance occurs, as proved in Section III-A. Moreover, as concluded in Section IV, group D implementations are not adequate for delay compensation schemes. Therefore, they should only be employed when delay compensation is not required and frequency adaptation is needed in combination with a low value of the product $\omega_o T_s$. In these cases, their advantage in computational simplicity makes them an interesting solution, specially when low-cost digital devices are employed. From the whole study, the best alternatives among group D methods are $H^{\rm PR}_{\rm f\&b}(z)$, $H^{\rm VPI}_{\rm f\&b}(z)$, and $H^{\rm VPI}_{\rm b\&b}(z)$.

On the other hand, referring back to Section III-A, group E methods achieve an accurate resonant poles mapping. Furthermore, it is possible to provide frequency adaptation to group E expressions by calculating the coefficients as ω_o varies, as done in [33]. In this manner, the performance would be superior in terms of resonant poles displacement and stability, even when tracking high frequencies and employing low values of f_s. Nevertheless, it would require the online computation of a cosine function for each resonance in every sample, so the computational burden may increase significantly.

Among group E discretizations, the most appropriate from the point of view of stability have been demonstrated in Section III-B to be FOH, Tustin with prewarping and ZPM

in the case of $R^2(s)$, and the impulse invariant method for $R^1(s)$. However, ZPM is not adequate for implementing delay compensation, as proved in Section IV.

VI. Experimental Setup Description

The experimental setup consists of a single-phase APF prototype; the choice of implementing the resonant controllers for an APF is mainly based on the fact that it is an application very suitable for testing their performance when tracking different frequencies. These results can be extended to other single-phase and three-phase applications where a perfect tracking/rejection of references/disturbances is sought through resonant controllers. The goal of the laboratory/experimental setup is to prove the following main theoretical approaches.

1) A comparison among discretization methods, testing the ability of different strategies to provide a good tracking/rejection of harmonic references/disturbances by means of an accurate mapping of the resonant poles (Section VII-A).
2) Effectiveness of the discrete-time delay compensation provided by FOH, Tustin with prewarping, and impulse invariant. It is proved by checking the performance of resonant controllers tuned at high values of ω_o (Section VII-B).
3) Considering online frequency adaptation, assessment of computational burden difference between most accurate implementations and those that do not require online calculation of explicit trigonometric functions (Section VII-C).

The tests carried out in order to prove 1) and 2) are performed without online frequency adaptation, since the aspect under study is the accuracy of the implementations when the input frequency is fixed and well known, so the resonant controllers are implemented with constant coefficients (calculated offline). Actually, ω_o should have a fixed value during these tests, so the different implementations are compared under the same conditions. Frequency-adaptive resonant controllers are implemented for the last experiment, which provides a comparison in terms of computational effort.

It is not intended to provide a comparison between $H^{\mathrm{PR}}(s)$ and $H^{\mathrm{VPI}}(s)$ controllers. This kind of study has already been presented in other papers [17], [23].

Fig. 11 shows the tested single-phase APF prototype. The APF is an insulated gate bipolar transistor (IGBT) based voltage source converter (VSC) connected to the point of common coupling (PCC) through the interfacing inductor L_f. The equivalent series resistance (R_f) of this inductor has been measured and taken into account in the modeling of the plant. A programmable load (Hocherl & Hackl ZSAC426) is connected in parallel to the APF. This load allows to specify the demanded current harmonic content up to the 15th harmonic. Table IX shows the values of the power circuit components. The variable f_{sw} is the IGBTs switching frequency. A programmable ac source (Chroma 61501) has been employed.

The control has been implemented in a prototyping platform (dSpace DS1104), which includes a Power PC MPC8240 (PPC) and a Texas Instruments TMS320F240 DSP. The PPC is a 64-bit floating-point processor with a CPU clock running at 250 MHz. The algorithms are designed using MATLAB/Simulink and the real-time interface (RTI) toolbox. The PPC executes all tasks, but the pulsewidth modulation (PWM) signals generation, which is done by the DSP. Some blocks, such as the moving average filters of the extraction algorithm and the frequency-adaptive resonant controllers, have been implemented by S-functions written in C language to optimize the execution times, as done in [16].

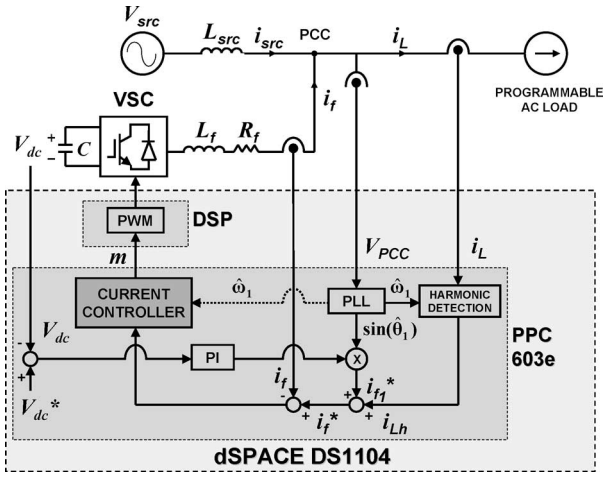

Fig. 11. APF laboratory prototype circuit and controller.

TABLE IX
Power Circuit Values

Parameter	Value
V_{dc}^*	220 V
$V_{src_{rms}}$	110 V
C	3.3 mF
L_f	5 mH
R_f	0.5 Ω
L_{src}	50 μH
$f_{sw} = f_s$	10 kHz

The discrete-time solver has been set at $f_s = 10$ kHz. The goals of the digital controller are to compensate for the selected load harmonic currents (i_{Lh}) and to keep constant the dc-link voltage (V_{dc}). The proposed controller works as follows.

1) The instantaneous load current (i_L) is detected.
2) The reference of the harmonic currents to compensate (i_{Lh}) are extracted from i_L by means of digital signal processing. The method that is proposed in [34] to identify the fundamental current (i_{L1}) has been employed, so $i_{Lh} = i_L - i_{L1}$.
3) The reference fundamental current ($i_{f_1}^*$), calculated to maintain V_{dc}, is obtained by means of a PI controller and the in-phase signal from the phase-locked loop (PLL) ($\hat{\theta}_1$) [35].
4) The total reference of current for the APF (i_f*) is calculated as $i_{Lh} + i_{f_1}^*$.
5) The current regulator [$G_c(z)$] assures that $\Delta i_f = i_f^* - i_f$ is zero in steady state.
6) The PLL estimates the fundamental frequency ($\hat{\omega}_1$) in order to adapt the harmonic identification algorithm and,

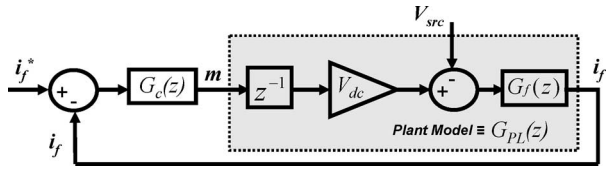

Fig. 12. Current control closed loop.

in the tests of computational burden, also the resonant controllers.

The resonant controllers are implemented in the stationary frame, which is a common choice due to the perfect tracking of both sequences and the lack of coordinates transformations [1], [13], [14], [20]–[22]. It is also an interesting alternative to implement them in SRF, as done in [7], [15]–[17], [22], [23]. However, the effects of discretization are analogous in both cases, so only one of these approaches is needed in this paper.

A. Modeling of the Plant

Fig. 12 depicts the current control system with the PR controller and the model of the plant. The discrete-time model of the plant $[G_{PL}(z)]$ has been modeled including the computational delay (z^{-1}) and the PWM converter operation [36], [37]. The PWM converter reference (m) is kept constant over each sampling interval, so the power converter can be assumed to be a ZOH circuit. Therefore, the inductive filter discrete-time model $[G_f(z)]$ should be obtained through the ZOH method [36], [37]:

$$G_f(s) = \frac{1}{sL_f + R_f} \overset{\text{zoh}}{\rightarrow} G_f(z) = \frac{1}{R_f} \frac{1 - e^{-R_f T_s / L_f}}{z - e^{-R_f T_s / L_f}}. \quad (7)$$

B. Tuning of H^{PR} Controllers

The controller $H_k^{\text{PR}}(s)$ for each harmonic k can be defined as

$$H_k^{\text{PR}}(s) = K_{P_k} + K_{I_k} R_k^1(s). \quad (8)$$

The individual K_{P_k} gains may be added, so only a single gain K_{P_T} should be adjusted [14], [17]. In this manner, when the current controller $G_c(s)$ is based on $H^{\text{PR}}(s)$, it takes the form

$$G_c(s) = \sum_{k=1,3,\ldots}^{n} H_k^{\text{PR}}(s) = K_{P_T} + \sum_{k=1,3,\ldots}^{n} K_{I_k} R_k^1(s) \quad (9)$$

with n being the highest harmonic order to be compensated. Two values of n will be employed in the experiments: 15 and 61.

The parameters of H_k^{PR} can be tuned according to the open-loop frequency response [14]. The proportional gain K_{P_T} establishes the frequency at which the gain is 0 dB, if no resonant controllers are considered. Thus, its value is very related to the stability of the system [14], and it is tuned to provide an adequate phase margin. Furthermore, resonant controllers without delay compensation should be only included within the bandwidth given by K_{P_T}; otherwise, stability is not assured [30]. On the other hand, the transient time is reduced as the proportional gain increases [14].

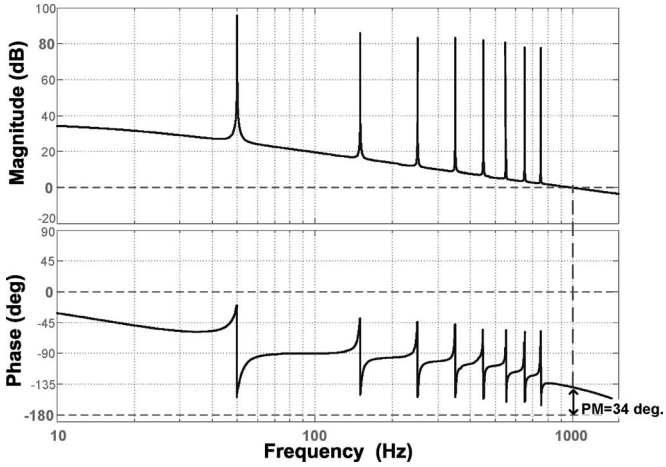

Fig. 13. Open-loop Bode diagram of $G_c(z)G_{PL}(z)$ for PR controllers with $n = 15$.

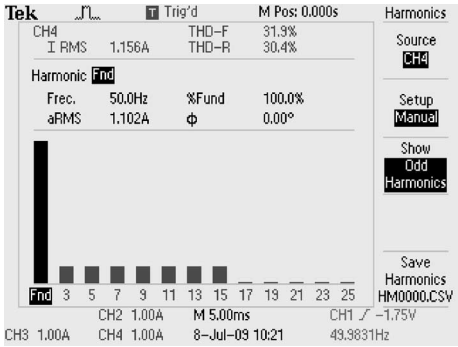

Fig. 14. Spectrum of programmed load current i_L to test the effect of resonant poles displacement [both for $H^{\text{PR}}(z)$ and $H^{\text{VPI}}(z)$]. THD= 31.9%.

A value of $K_{P_T} = 32$ has been selected so that a bandwidth of about 1 kHz is achieved. Consequently, it is possible to employ resonant controllers without delay compensation for $n = 15$, which is necessary for some of the experiments. Fig. 13 depicts the open-loop frequency response obtained after the tuning process for $n = 15$. The phase margin results in 34°, assuring stability.

Concerning K_{I_k} tuning, the main aspect that should be considered is the compromise between selective filtering and dynamic response [30], [38]. An identical integral gain has been selected for each harmonic k in order to achieve the same bandwidth for all of them. In this manner, an equivalent trade-off between selectivity and transient response is assured for each resonant frequency. Indeed, it is a common practice to tune PR controllers with identical gains K_{I_k} for all harmonics [14], [24], [39]. Furthermore, as the selectivity becomes independent of the harmonic order, it will be possible to assess in the experiments the dependence of the resonance deviation on k, which is one of the main objectives of the experiments. Taking into account all these aspects, a value of $K_{I_k} = 2000$ has been selected. It can be mentioned that this is equivalent to an integral gain of 1000 in an SRF PI controller [21].

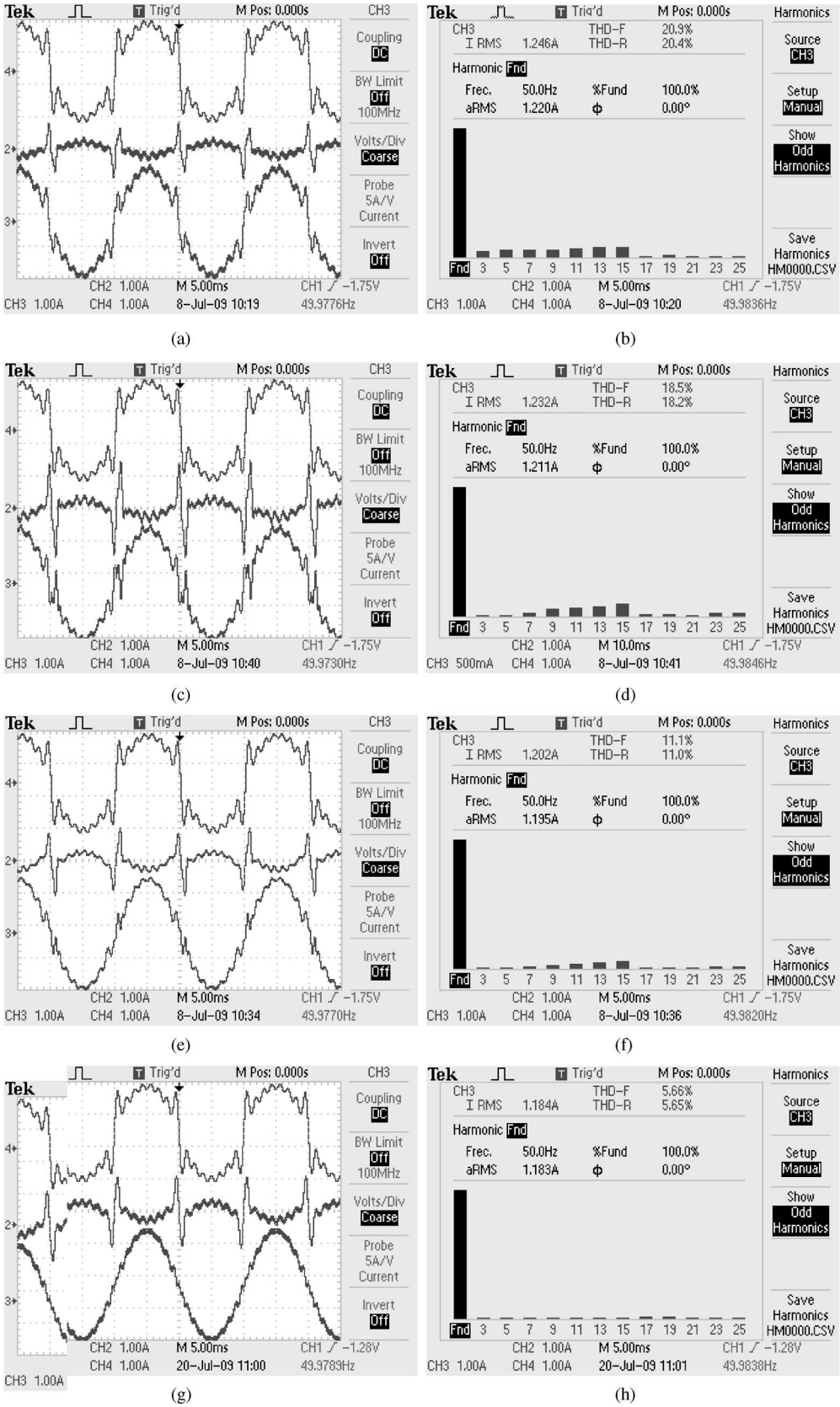

Fig. 15. Steady-state currents and spectrum of $i_{\rm src}$ for different discrete implementations of $H^{\rm PR}(s)$, with $n = 15$ and $f_1 = 50$ Hz. Ch2 is i_f, Ch3 is $i_{\rm src}$, and Ch4 is i_L. (a) Steady-state currents for only proportional current controller. (b) Spectrum of $i_{\rm src}$ shown in Fig. 15(a). THD $= 20.9\%$. (c) Steady-state currents for $H^{\rm PR}_{\rm t}(z)$ implementation. (d) Spectrum of $i_{\rm src}$ shown in Fig. 15(c). THD $= 18.5\%$. (e) Steady-state currents for $H^{\rm PR}_{\rm f\&b}(z)$ implementation. (f) Spectrum of $i_{\rm src}$ shown in Fig. 15(e). THD $= 11.1\%$. (g) Steady-state currents for $H^{\rm PR}_{\rm imp}(z)$ implementation. (h) Spectrum of $i_{\rm src}$ shown in Fig. 15(g). THD $= 5.66\%$.

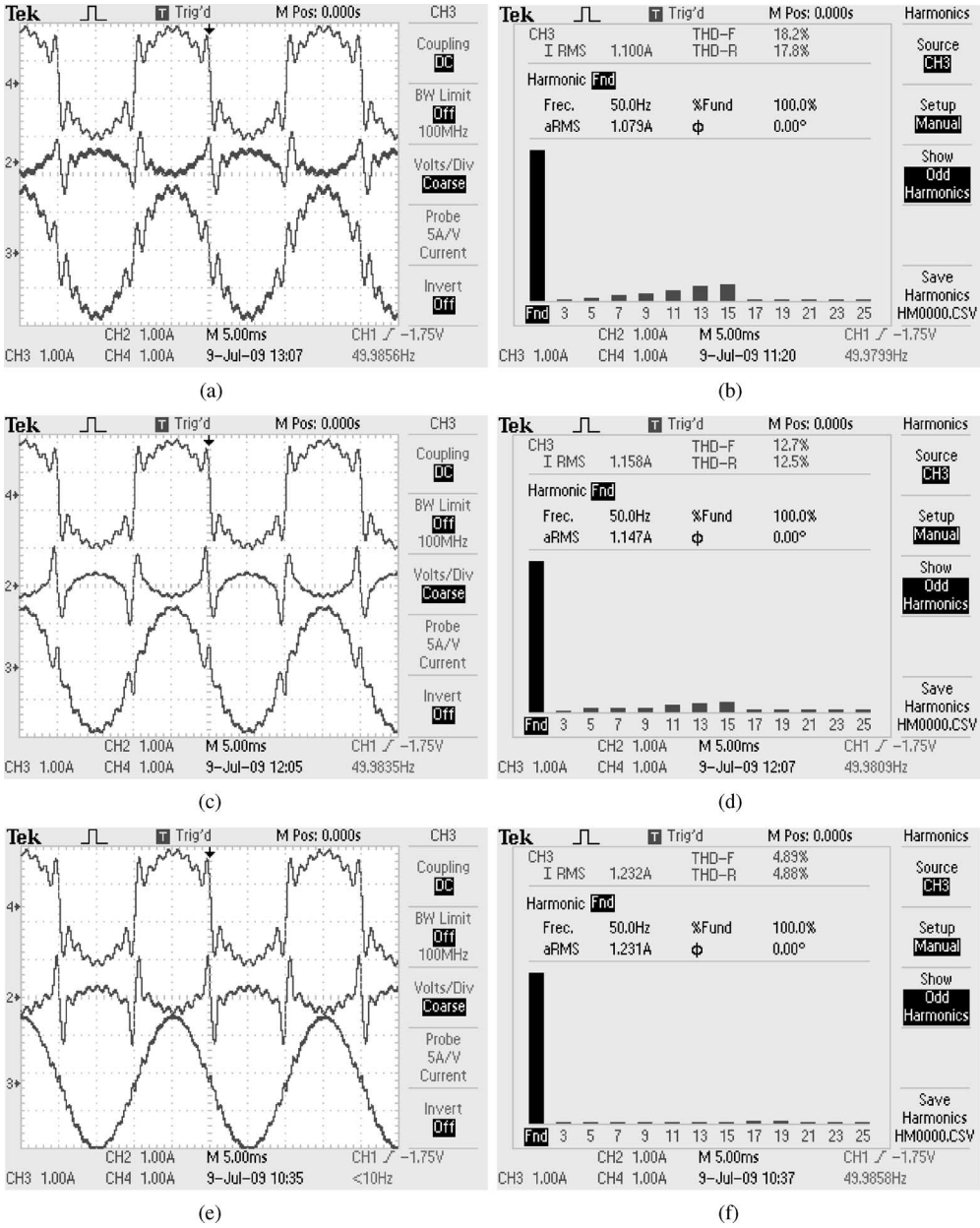

Fig. 16. Steady-state currents and spectrum of $i_{\rm src}$ for different discrete implementations of $H^{\rm VPI}(s)$, with $n = 15$ and $f_1 = 50$ Hz. Ch2 is i_f, Ch3 is $i_{\rm src}$ and Ch4 is i_L. (a) Steady-state currents for $H^{\rm VPI}_{t-t}(z)$. (b) Spectrum of $i_{\rm src}$ shown in Fig. 16(a). THD $= 18.2\%$. (c) Steady-state currents for $H^{\rm VPI}_{\rm f\&b}(z)$ implementation. (d) Spectrum of $i_{\rm src}$ shown in Fig. 15(c). THD $= 12.7\%$. (e) Steady-state currents for $H^{\rm VPI}_{\rm imp-tp}(z)$. (f) Spectrum of $i_{\rm src}$ shown in Fig. 15(e). THD $= 4.89\%$.

It should be remarked that the resonant peak at the fundamental component provides total disturbance (fundamental component of $V_{\rm src}$) rejection, so a feedforward compensation is not needed [13], [24].

C. Tuning of $H^{\rm VPI}$ Controllers

The individual controller $H^{\rm VPI}_k(s)$ for each harmonic k is expressed as

$$H^{\rm VPI}_k(s) = K_{P_k} R^2_k(s) + K_{I_k} R^1_k(s). \tag{10}$$

The total current controller is

$$G_c(s) = \sum_{k=1,3,\ldots}^{n} H^{\rm VPI}_k(s). \tag{11}$$

The gains of $H^{\rm VPI}_k$ have been tuned according to the indications exposed in [16] and [17].

1) In order to cancel the cross coupling caused by the *R–L* filter, K_{I_k} is selected as $K_{P_k} R_f / L_f$.
2) There is a direct relation between K_{P_k} and the width of the peaks, determining the selectivity and the transient time. This parameter should be set in order to provide a given bandwidth centered at the resonant frequencies. $K_{P_k} =$

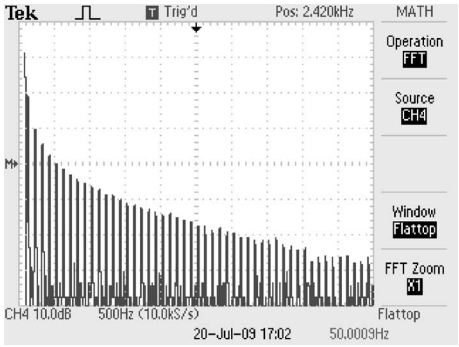

Fig. 17. Spectrum of programmed load current i_L for the tests of discrete-time delay compensation.

0.5 and $K_{I_k} = 50$ have been chosen to achieve a closed-loop bandwidth of 16 Hz at each resonance frequency $k\omega_1$, so an adequate tradeoff between selectivity and transient response is achieved.

3) So as to obtain the same bandwidth for all controllers, identical gains K_{P_k} and K_{I_k} are selected for each harmonic k, as proposed in [16] and [17]. Moreover, it is necessary to employ the same gains for each resonance frequency in order to appreciate how the resonant poles deviation increases with the harmonic order.

VII. Experimental Results

A. Comparison of Steady-State Error Provided by Discrete-Time Implementations

The load current i_L has been programmed with uniform harmonic spectrum for odd values between the 3rd and 15th order, as depicted in Fig. 14. It should be noted that THD-F, which means referred to fundamental, corresponds with the standard definition of THD. In this manner, the uniform spectrum leads to a THD of 31.9%. In most real applications, low harmonics exhibit higher amplitude, but in this paper, i_L has been chosen in this manner to make possible the comparison of the performance as the harmonic order rises. The number of harmonics could be increased by performing compensation of the computational delay, but it is not done in this test due to the following reasons.

1) Results obtained with $n = 15$ will be enough to prove the effect of discretization on the resonant frequency. The error expected for low-order harmonics is already considerable (exposed in Section III-A), so testing resonant controllers tuned for higher harmonics would not contribute any additional information.
2) If higher harmonics were to be compensated, delay compensation should be implemented in order to assure stability of the resonant terms. However, as exposed in Section IV, this would change the form of the original continuous transfer function to (4); thus, additional effects of the discretization would also affect the performance apart from the resonant poles displacement.

1) Steady-State Error of $H^{\mathrm{PR}}(s)$ Discretizations: Fig. 15 illustrates steady-state currents and corresponding spectrum of

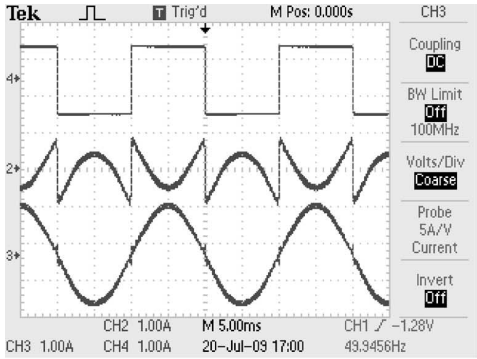

(a)

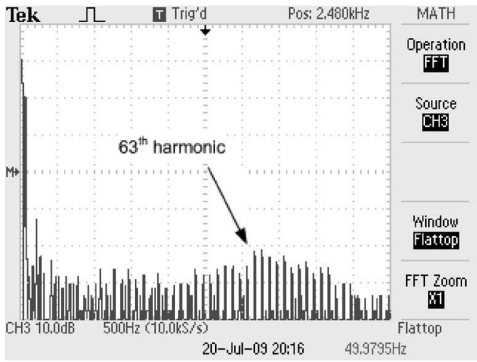

(b)

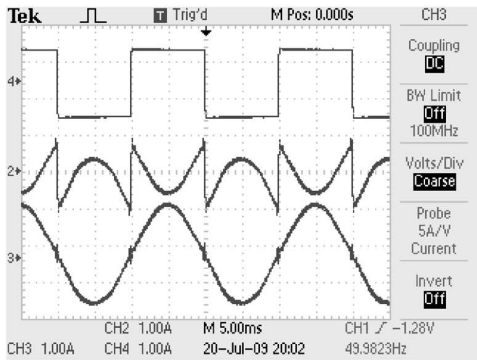

(c)

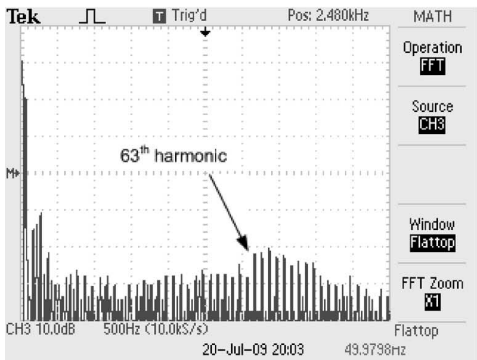

(d)

Fig. 18. Steady-state currents and spectrum of i_{src} when implementing digital compensation of the computational delay, with $N = 2$, $n = 61$, and $f_1 = 50$ Hz. Ch2 is i_f, Ch3 is i_{src}, and Ch4 is i_L. (a) Steady-state currents for $H_{\mathrm{imp}}^{\mathrm{PR}^d}(z)$. (b) Spectrum of i_{src} shown in Fig. 18(b). (c) Steady-state currents for $H_{\mathrm{imp-tp}}^{\mathrm{VPI}^d}(z)$. (d) Spectrum of i_{src} shown in Fig. 18(d).

TABLE X
IMPLEMENTATION CODE FOR THE TESTS OF COMPUTATIONAL BURDEN

PR controllers			VPI controllers		
$R^1_{\text{f\&b}}$	y[0]=x[1]*Ts+y[0];	58	$H^{\text{VPI}}_{\text{f\&b}}$	x[0]=x[2]*Ts+x[0];	61
	x[0]=w[0]*w[0]*y[0]*Ts+x[0];	59		x[1]=w[0]*w[0]*x[0]*Ts+x[1];	62
	x[1]=u[0]-x[0];	60		x[2]=u[0]-x[1];	63
				y[0]=Kp*x[2]+Ki*x[0];	64
R^1_{imp}	**b1=cos(w[0]*Ts);**	**68**	$H^{\text{VPI}}_{\text{imp-tp}}$	**b1=cos(w[0]*Ts);**	**72**
	y[0]=Ts*u[0]-b1*x[0]+2*b1*x[2]-x[1];	69		b2=0.5*Kp*(b1+1);	73
	x[0]=Ts*u[0];	70		y[0]=u[0]*(Ki*Ts+b2)-x[1]*(Ki*Ts*b1+2*b2)+x[0]*b2+2*x[3]*b1-x[2];	74
	x[1]=x[2];	71		x[0]=x[1];	75
	x[2]=y[0];	72		x[1]=u[0];	76
				x[2]=x[3];	77
				x[3]=y[0];	78

i_{src} for different discrete-time implementations of the PR current controller [$H^{\text{PR}}(s)$]. As expected from the theoretical analysis provided in Section III-A, the steady-state error caused by the pole displacement of the implementations of groups C and D is considerable and increases with the harmonic order, as shown in Fig. 15(d) and (f). Actually, for high-order harmonics, the i_{src} Fourier spectrum achieved by $R^1_{\text{f\&b}}(z)$ and $R^1_t(z)$ schemes is more similar to the one provided by a simple proportional controller [see Fig. 15(b)] than to the harmonic content achieved by $R^1_{\text{imp}}(z)$ [see Fig. 15(h)].

The latter provides almost complete rejection of load current harmonics, proving the accuracy of its resonant peaks locations. The THD values also reflect the large performance difference: its value for $R^1_{\text{f\&b}}(z)$ (THD $= 11.1\%$) and $R^1_t(z)$ (THD $= 18.5\%$), respectively, doubles and triples that of $R^1_{\text{imp}}(z)$ (THD $= 5.66\%$). Therefore, it is proved the superiority of group E methods for $R^1(z)$ implementation in terms of accuracy.

2) Steady-State Error of $H^{\text{VPI}}(s)$ Discretizations: Fig. 16 compares the steady-state currents and i_{src} spectrum obtained by the different stable groups of discretization methods when applied to $H^{\text{VPI}}(s)$: C, D, and E. As shown in Fig. 16(e), group E achieves a high rejection of all programmed harmonics between $k = 3$ and $k = 15$, due to an accurate mapping of the resonant poles. On the contrary, the other groups fail to track with unitary gain the harmonic references. They produce a difference in the resonant frequency that increases with the harmonic order, thus causing steady-state error. This fact can be also appreciated in the THD values: it rises from 4.89% to 12.7% and 18.2% (groups E, D, and C, respectively). In sum, E techniques have been proved to provide a superior performance for $H^{\text{VPI}}(s)$ controllers in terms of resonant poles accuracy.

B. Test of Discrete-Time Delay Compensation

The effectiveness of the digital implementations of the delay compensation will be tested by checking their stability when compensating high-order harmonics. For this reason, I_L has been programmed as a square wave with rise time and fall time of 39 μs. It contains a very demanding spectrum of odd harmonics up to high frequencies. Its harmonic content can be observed in Fig. 17. In these experiments, the fast Fourier transform (FFT) tool of the oscilloscope math mode has been employed instead of the application used in the previous tests. This is because of the fact that the latter is only able to show harmonics up to $k = 49$, whereas the former is only limited by the bandwidth of the oscilloscope.

The number of samples compensated has been set at $N = 2$, since it was concluded in [23] to be the optimum value.

Resonant controllers will be tuned at each odd harmonic between $k = 1$ and $k = n = 61$. Higher frequencies could be tracked, but the precision would become really low, as the number of samples in a period gets too small. In any case, $n = 61$ is considered enough for proving robustness of current controllers [17].

It should be noted that the aim of the experiment is not a proposal for an industrial prototype, but to provide a study about the accuracy of the resonant poles locations and the delay compensation achieved by several discretization methods. The main reason to implement resonant controllers tuned at such high frequencies is to serve as an useful test for applications in which tracking of high frequencies is common, such as aeronautic APFs or torque ripple minimization in high-speed PM drives. Obviously, so many resonant controllers are not required in these cases, but the results provided confirm that there would be no problems of accuracy when few resonant controllers tuned at high frequencies are implemented.

1) $H^{\text{PR}}(z)$ Delay Compensation: If a delay compensation method is not included, $H^{\text{PR}}(s)$ controllers are inherently unstable starting from the 19th harmonic [17], [23]. Fig. 18(a) shows the steady-state currents obtained by $R^{1^d}_{\text{imp}}(z)$ implementation, proving its stability. Therefore, it can be stated that the discrete-time delay compensation fulfills its mission of providing stability to the resonant controllers. The same results have been obtained by $R^{1^d}_{\text{foh}}(z)$ and $R^{1^d}_{\text{tp}}(z)$.

Moreover, from the spectrum of i_{src} shown in Fig. 18(b), it can be also concluded that the mapping of the resonant poles of group E is still accurate for such high values of ω_o. Indeed, a similar amplitude is achieved for the higher values of k when compared to the lower. It should be remarked that the harmonic components are not entirely eliminated mainly due to the error of the current sensors.

It should be also noted that the discretization of the controllers including the computational delay does not affect the denominator of each group, so the resonant poles will be the same for each group indistinctly if the delay compensation is included or

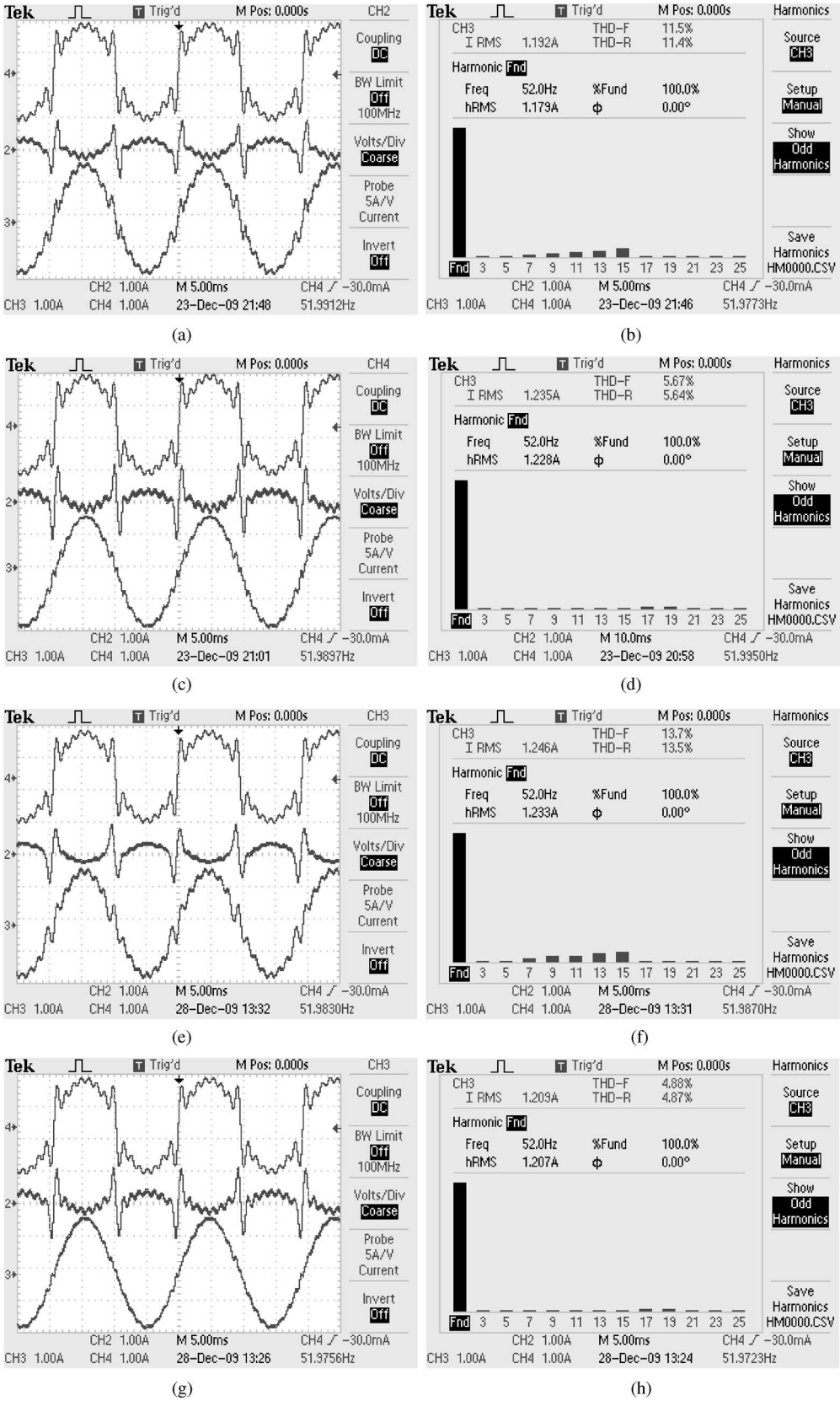

Fig. 19. Steady-state currents and spectrum of $i_{\rm src}$ for frequency-adaptive implementations of Table X, with $n = 15$ and $f_1 = 52$ Hz. Ch2 is i_f, Ch3 is $i_{\rm src}$, and Ch4 is i_L. (a) Steady-state currents for $H^{\rm PR}_{\rm f\&b}(z)$ implementation. (b) Spectrum of $i_{\rm src}$ shown in Fig. 19(a). THD $= 11.5\%$. (c) Steady-state currents for $H^{\rm PR}_{\rm imp}(z)$ implementation. (d) Spectrum of $i_{\rm src}$ shown in Fig. 19(c). THD $= 5.67\%$. (e) Steady-state currents for $H^{\rm VPI}_{\rm f\&b}(z)$ implementation. (f) Spectrum of $i_{\rm src}$ shown in Fig. 19(e). THD $= 13.7\%$. (g) Steady-state currents for $H^{\rm VPI}_{\rm imp-tp}(z)$ implementation. (h) Spectrum of $i_{\rm src}$ shown in Fig. 19(g). THD $= 4.88\%$.

not. That is the reason why these experimental results can be also considered as an extension of the results of Section VII-A, in the sense of proving the correct mapping of the poles for harmonics higher than $k = 15$.

The average execution time of this experiment has been $24.6\ \mu$s (whole control). The PR current control, which includes 31 resonant controllers with fixed coefficients, employs $15.2\ \mu$s.

2) $H^{\mathrm{VPI}}(z)$ Delay Compensation: The VPI controller is not able to compensate harmonics higher than 37th unless delay compensation is implemented [17]. As can be observed in Fig. 18(c), the proposed implementation of digital delay compensation for $H^{\mathrm{VPI}}(z)$ is capable of providing stability even to really high harmonic orders. Therefore, its suitability has been satisfactorily proved. The results shown in these figures have been obtained with $R^{1^d}_{\mathrm{imp}}(z)$ and $R^{2^d}_{\mathrm{tp}}(z)$, but identical results have been also achieved with $R^{1^d}_{\mathrm{foh}}(z)$, $R^{1^d}_{\mathrm{tp}}(z)$, $R^{2^d}_{\mathrm{foh}}(z)$, and $R^{2^d}_{\mathrm{tp}}(z)$.

Fig. 18(d) also demonstrates the accuracy of the resonant poles locations provided by group E in the case of $H^{\mathrm{VPI}^d}(z)$.

The average execution time of this experiment has been $25.9\ \mu$s (whole control). The PR current control employs $16.5\ \mu$s. It should be noted that these execution times are quite reduced due to the powerful microprocessor employed (250 MHz clock rate) and the fact that constant coefficients (calculated offline) were employed in the resonant controllers. The effect of online calculation of coefficients involving trigonometric functions is assessed in the next section.

C. Comparison of Computational Burden

In the previous experiments, the discretization methods that provide the best accuracy have been established. However, these implementations require online computation of trigonometric functions, as opposed to the schemes based on two integrators. In this manner, it can be said that there exists a tradeoff between accuracy and resource-consumption, when frequency adaptation is required. Therefore, it is interesting to assess the difference in execution time between groups D and E implementations.

One implementation of group D and one of group E have been chosen, both for the PR and the VPI controllers, to perform the comparison of execution time: $H^{\mathrm{PR}}_{\mathrm{f\&b}}$, $H^{\mathrm{PR}}_{\mathrm{imp}}$, $H^{\mathrm{VPI}}_{\mathrm{f\&b}}$, and $H^{\mathrm{VPI}}_{\mathrm{imp-tp}}$. Results with other implementations of the same groups would be very similar due to the fact that the most critical operation is the cosine calculation, which is necessary in all methods of group E and none of group D. The most significant instructions of the code of the tested controllers (S-functions in C language) are shown in Table X.

Seven resonant controllers of each type are implemented ($n = 15$), and the load current is programmed with a uniform spectrum up to the 15th harmonic, as done in the experiments of Section VII-A. Fig. 19 depicts the currents obtained by the frequency-adaptive implementations of Table X, with $f_1 = 52$ Hz. Fig. 19 proves the effectiveness of Table X code to implement the original transfer functions even in presence of frequency deviations.

Table XI shows the average execution times of Table X controllers running in steady state. These results corroborate the observations posed in Section V concerning the simplicity of the implementations based on two integrators. From Table XI, the schemes of group D permit to reduce the execution time by a factor of approximately 4. This result is explained by the fact that the RTI implements, by default, sine/cosine terms by means of high order (15th) Taylor series, which demand a lot of PPC clock cycles (low-level instructions); whereas, methods based on two discrete integrators approximate the cosine function as a Taylor series of second order (as shown in Table III) with much less low-level instructions. Consequently, the best tradeoff depends on available resources and required accuracy.

TABLE XI
EXECUTION TIME OF THE CONTROLLERS IN THE TESTS OF STEADY-STATE ERROR

Controller (n=15)	Current control execution time	Whole control execution time
$H^{\mathrm{PR}}_{\mathrm{f\&b}}$	2.5 μs	11.9 μs
$H^{\mathrm{PR}}_{\mathrm{imp}}$	8.3 μs	17.7 μs
$H^{\mathrm{VPI}}_{\mathrm{f\&b}}$	2.7 μs	12.1 μs
$H^{\mathrm{VPI}}_{\mathrm{imp-tp}}$	8.6 μs	18.0 μs

VIII. CONCLUSION

An exhaustive analysis of the importance of the discrete-time implementations of resonant controllers is contributed in this paper. Some important outcomes should be taken into account when implementing digital resonant controllers.

1) Forward Euler and backward Euler methods are not suitable for discretizing resonant controllers, since they map the poles out of the unit circumference. On the other hand, the rest of the implementations are able to achieve infinite gain in open-loop.
2) The discrete-time implementations based on the Tustin transformation [28] and the ones based on two integrators [8], [13], [15], [23]–[25] produce a significant steady-state error due to resonant poles displacement. This error increases with the sampling period and the harmonic order. Therefore, they are not recommended for applications in which high frequencies should be tracked. However, this deviation can be negligible when low frequencies (low $\omega_o T_s$), such as fundamental components and low-order harmonics, are tracked. Furthermore, the schemes based on two integrators, which approximate a cosine function by a second-order Taylor series, permit to reduce the computational burden with respect to more accurate implementations. Consequently, their simplicity may be advantageous in cases in which their steady-state error is acceptable and frequency adaptation is required.
3) Implementations obtained by ZOH, FOH [30], impulse invariant, Tustin with prewarping [29], [31], and ZPM provide an accurate location of the resonant peaks even for high frequencies and reduced sampling rates. Consequently, they are more suitable to achieve zero steady-state error. When frequency adaptation is implemented, the online calculation of trigonometric functions is required, which may be very resource-consuming.

4) Concerning PR controllers, the discrete transfer function obtained by the impulse invariant method is the most optimal among these methods, since its zeros distribution causes less phase lag. Thus, it improves stability. On the other hand, ZOH is the most unfavorable of them, because it introduces a delay near the resonant frequency.
5) Concerning VPI controllers, they can be separated in two resonant terms, one of which is identical to the resonant term included in PR controllers. Therefore, the statements from the previous point can be also applied to this equivalent resonant term. In relation with the other resonant term included in the VPI controller, either FOH, Tustin with prewarping, or ZPM are adequate options. On the contrary, ZOH and impulse invariant may cause instability.
6) The methods that provide an effective discrete-time implementation of the delay compensation are FOH, Tustin with prewarping, and impulse invariant for either resonant term. Other techniques can easily lead to instability due to the large difference they produce in the phase response near the resonant frequency.

Experimental results obtained with an APF laboratory prototype validate the most important outcomes of the theoretical analysis. In sum, it has been proved that the choice of the discretization method is a crucial aspect for resonant controllers, and the most suitable alternatives have been established. The effectiveness of the proposed optimum implementations of the digital delay compensation have been tested by compensating odd harmonics up to the 61th order.

REFERENCES

[1] A. Timbus, M. Liserre, R. Teodorescu, P. Rodriguez, and F. Blaabjerg, "Evaluation of current controllers for distributed power generation systems," *IEEE Trans. Power Electron.*, vol. 24, no. 3, pp. 654–664, Mar. 2009.

[2] A. V. Timbus, M. Ciobotaru, R. Teodorescu, and F. Blaabjerg, "Adaptive resonant controller for grid-connected converters in distributed power generation systems," in *Proc. 21st Annu. IEEE Appl. Power Electron. Conf. Expo. (APEC 2006),* Mar., pp. 1601–1606.

[3] Y. W. Li, F. Blaabjerg, D. M. Vilathgamuwa, and P. C. Loh, "Design and comparison of high performance stationary-frame controllers for DVR implementation," *IEEE Trans. Power Electron.*, vol. 22, no. 2, pp. 602–612, Mar. 2007.

[4] Y. W. Li, P. C. Loh, F. Blaabjerg, and D. M. Vilathgamuwa, "Investigation and improvement of transient response of DVR at medium voltage level," *IEEE Trans. Ind. Appl.*, vol. 43, no. 5, pp. 1309–1319, Sep./Oct. 2007.

[5] M. Liserre, R. Teodorescu, and F. Blaabjerg, "Stability of photovoltaic and wind turbine grid-connected inverters for a large set of grid impedance values," *IEEE Trans. Power Electron.*, vol. 21, no. 1, pp. 263–272, Jan. 2006.

[6] P. Zhou, Y. He, and D. Sun, "Improved direct power control of a DFIG-based wind turbine during network unbalance," *IEEE Trans. Power Electron.*, vol. 24, no. 11, pp. 2465–2474, Nov. 2009.

[7] M. Liserre, R. Teodorescu, and F. Blaabjerg, "Multiple harmonics control for three-phase grid converter systems with the use of PI-RES current controller in a rotating frame," *IEEE Trans. Power Electron.*, vol. 21, no. 3, pp. 836–841, May 2006.

[8] R. Teodorescu, F. Blaabjerg, U. Borup, and M. Liserre, "A new control structure for grid-connected LCL PV inverters with zero steady-state error and selective harmonic compensation," *Proc. 19th Annu. IEEE Appl. Power Electron. Conf. Expo. (APEC 2004)*, vol. 1, pp. 580–586.

[9] S.-Y. Park, C.-L. Chen, and J. S. J. Lai, "A wide range active and reactive power flow controller for a solid oxide fuel cell power conditioning system," *IEEE Trans. Power Electron.*, vol. 23, no. 6, pp. 2703–2709, Nov. 2008.

[10] S. Y. Park, C. L. Chen, J. S. Lai, and S. R. Moon, "Admittance compensation in current loop control for a grid-tie LCL fuel cell inverter," *IEEE Trans. Power Electron.*, vol. 23, no. 4, pp. 1716–1723, Jul. 2008.

[11] A. Dell'Aquila, M. Liserre, V. G. Monopoli, and P. Rotondo, "Overview of PI-based solutions for the control of DC buses of a single-phase h-bridge multilevel active rectifier," *IEEE Trans. Ind. Appl.*, vol. 44, no. 3, pp. 857–866, May 2008.

[12] L. Asiminoaei, F. Blaabjerg, S. Hansen, and P. Thogersen, "Adaptive compensation of reactive power with shunt active power filters," *IEEE Trans. Ind. Appl.*, vol. 44, no. 3, pp. 867–877, May 2008.

[13] S. Fukuda and T. Yoda, "A novel current-tracking method for active filters based on asinusoidal internal model [for PWM invertors]," *IEEE Trans. Ind. Appl.*, vol. 37, no. 3, pp. 888–895, May/Jun. 2001.

[14] X. Yuan, W. Merk, H. Stemmler, and J. Allmeling, "Stationary-frame generalized integrators for current control of active power filters with zero steady-state error for current harmonics of concern under unbalanced and distorted operating conditions," *IEEE Trans. Ind. Appl.*, vol. 38, no. 2, pp. 523–532, Mar./Apr. 2002.

[15] R. I. Bojoi, G. Griva, V. Bostan, M. Guerriero, F. Farina, and F. Profumo, "Current control strategy for power conditioners using sinusoidal signal integrators in synchronous reference frame," *IEEE Trans. Power Electron.*, vol. 20, no. 6, pp. 1402–1412, Nov. 2005.

[16] C. Lascu, L. Asiminoaei, I. Boldea, and F. Blaabjerg, "High performance current controller for selective harmonic compensation in active power filters," *IEEE Trans. Power Electron.*, vol. 22, no. 5, pp. 1826–1835, Sep. 2007.

[17] C. Lascu, L. Asiminoaei, I. Boldea, and F. Blaabjerg, "Frequency response analysis of current controllers for selective harmonic compensation in active power filters," *IEEE Trans. Ind. Electron.*, vol. 56, no. 2, pp. 337–347, Feb. 2009.

[18] Y. W. Li, D. M. Vilathgamuwa, and P. C. Loh, "Robust control scheme for a microgrid with PFC capacitor connected," *IEEE Trans. Ind. Appl.*, vol. 43, no. 5, pp. 1172–1182, Sep./Oct. 2007.

[19] M.-C. Chou and C.-M. Liaw, "Development of robust current 2-DOF controllers for a permanent magnet synchronous motor drive with reaction wheel load," *IEEE Trans. Power Electron.*, vol. 24, no. 5, pp. 1304–1320, May 2009.

[20] D. N. Zmood, D. G. Holmes, and G. H. Bode, "Frequency-domain analysis of three-phase linear current regulators," *IEEE Trans. Ind. Appl.*, vol. 37, no. 2, pp. 601–610, Mar./Apr. 2001.

[21] D. N. Zmood and D. G. Holmes, "Stationary frame current regulation of PWM inverters with zero steady-state error," *IEEE Trans. Power Electron.*, vol. 18, no. 3, pp. 814–822, May 2003.

[22] A. Garcia-Cerrada, P. Roncero-Sanchez, P. Garcia-Gonzalez, and V. Feliu-Batlle, "Detailed analysis of closed-loop control of output-voltage harmonics in voltage-source inverters," in *Proc. Inst. Electr. Eng. Electric Power Appl.*, vol. 151, no. 6, pp. 734–743, Nov. 2004.

[23] L. Limongi, R. Bojoi, G. Griva, and A. Tenconi, "Digital current-control schemes," *IEEE Ind. Electron. Mag.*, vol. 3, no. 1, pp. 20–31, Mar. 2009.

[24] R. Teodorescu, F. Blaabjerg, M. Liserre, and P. C. Loh, "Proportional-resonant controllers and filters for grid-connected voltage-source converters," in *Proc. Inst. Electr. Eng., Electric Power Appl.*, vol. 153, no. 5, pp. 750–762, Sep. 2006.

[25] F. J. Rodriguez, E. Bueno, M. Aredes, L. G. B. Rolim, F. A. S. Neves, and M. C. Cavalcanti, "Discrete-time implementation of second order generalized integrators for grid converters," in *Proc. 34th Annu. Conf. IEEE Ind. Electron. (IECON 2008)*, Orlando, FL, Nov., pp. 176–181.

[26] H. T. Nagle and C. L. Phillips *Digital Control System Analysis and Design*, 3rd ed. Englewood Cliffs, NJ: Prentice-Hall, 1995.

[27] D. G. Holmes, T. A. Lipo, B. P. McGrath, and W. Y. Kong, "Optimized design of stationary frame three phase AC current regulators," *IEEE Trans. Power Electron.*, vol. 24, no. 11, pp. 2417–2426, Nov. 2009.

[28] M. J. Newman and D. G. Holmes, "Delta operator digital filters for high performance inverter applications," *IEEE Trans. Power Electron.*, vol. 18, no. 1, pp. 447–454, Jan. 2003.

[29] P. C. Tan, P. C. Loh, and D. G. Holmes, "High-performance harmonic extraction algorithm for a 25 kv traction power quality conditioner," in *Proc. Inst. Electr. Eng., Electric Power Appl.*, vol. 151, no. 5, pp. 505–512, Sep. 2004.

[30] R. P. Venturini, P. Mattavelli, P. Zanchetta, and M. Sumner, "Variable frequency adaptive selective compensation for active power filters," in *Proc. 4th IET Conf. Power Electron., Mach. Drives (PEMD 2008)*, Apr., pp. 16–21.

[31] L. Harnefors, "Implementation of resonant controllers and filters in fixed-point arithmetic," *IEEE Trans. Ind. Electron.*, vol. 56, no. 4, pp. 1273–1281, Apr. 2009.
[32] Y. A. R. Mohamed and E. F. El-Saadany, "Adaptive discrete-time grid-voltage sensorless interfacing scheme for grid-connected DG-inverters based on neural-network identification and deadbeat current regulation," *IEEE Trans. Power Electron.*, vol. 23, no. 1, pp. 308–321, Jan. 2008.
[33] X. Guillaud, P. Degobert, and R. Teodorescu, "Use of resonant controller for grid-connected converters in case of large frequency fluctuations," in *Proc. Eur. Conf. Power Electron. Appl.*, Aalborg, Denmark, Sep. 2007, pp. 1–8.
[34] F. D. Freijedo, J. Doval-Gandoy, O. Lopez, P. Fernandez-Comesana, and C. Martinez-Penalver, "A signal-processing adaptive algorithm for selective current harmonic cancellation in active power filters," *IEEE Trans. Ind. Electron.*, vol. 56, no. 8, pp. 2829–2840, Aug. 2009.
[35] J. Doval-Gandoy, A. Nogueiras, C. M. Penalver, and A. Lago, "Shunt active power filter with harmonic current control strategy," in *Proc. PESC*, 1998, pp. 1631–1635.
[36] M. Sedighy, S. Dewan, and F. Dawson, "A robust digital current control method for active power filters," *IEEE Trans. Ind. Appl.*, vol. 36, no. 4, pp. 1158–1164, Jul./Aug. 2000.
[37] H. Akagi, E. H. Watanabe, and M. Aredes, *Instantaneous Power Theory and Applications to Power Conditioning*, M. E. El-Hawari, Ed. New York: Wiley/IEEE Press, 2007.
[38] S. Buso and P. Mattavelli, *Digital Control in Power Electronics,* J. Hudgins, Ed. Seattle, WA: Morgan & Claypool Publishers, 2006.
[39] S. Fukuda and R. Imamura, "Application of a sinusoidal internal model to current control of three-phase utility-interface converters," *IEEE Trans. Ind. Electron.*, vol. 52, no. 2, pp. 420–426, Apr. 2005.

Alejandro G. Yepes (S'09) received the M.Sc. degree in 2009 from the University of Vigo, Vigo, Spain, where he is currently working toward the Ph.D. degree in the Department of Electronic Technology.

Since 2008, he has been with the Department of Electronics Technology, University of Vigo. His current research interests include switching power converters, grid-connected converters, control of ac drives, and power quality problems.

Francisco D. Freijedo (M'07) received the M.Sc. degree in physics from the University of Santiago de Compostela, Santiago de Compostela, Spain, in 2002, and the Ph.D. degree from the University of Vigo, Vigo, Spain, in 2009.

Since 2005, he has been an Assistant Professor in the Department of Electronics Technology, University of Vigo. His current research interests include quality problems, grid-connected switching converters, ac power conversion, and flexible ac transmission systems.

Jesús Doval-Gandoy (M'99) received the M.Sc. degree from the Polytechnic University of Madrid, Madrid, Spain, in 1991, and the Ph.D. degree from the University of Vigo, Vigo, Spain, in 1999.

From 1991 to 1994, he worked at industry. He is currently an Associate Professor in the Department of Electronics Technology, University of Vigo. His research interests include the areas of ac power conversion.

Óscar López (M'05) received the M.Sc. and Ph.D. degrees from the University of Vigo, Vigo, Spain, in 2001 and 2009, respectively.

Since 2004, he has been an Assistant Professor in the Department of Electronics Technology, University of Vigo. His current research interests include the areas of ac power switching converters technology.

Jano Malvar (S'09) received the M.Sc. degree in 2007 from the University of Vigo, Vigo, Spain, where he is currently working toward the Ph.D. degree in the Department of Electronic Technology.

Since 2007, he has been with the Department of Electronics Technology, University of Vigo. His current research interests include switching power converters, grid-connected converters, flexible ac transmission systems, and power quality problems.

Pablo Fernández-Comesaña (S'09) received the M.Sc. degree in 2007 from the University of Vigo, Vigo, Spain, where he is currently working toward the Ph.D. degree in the Department of Electronic Technology.

Since 2007, he has been with the Department of Electronics Technology, University of Vigo. His current research interests include switching power converters, grid-connected converters, flexible ac transmission systems, and power quality problems.